FOSSIL ENERGY

DOE/BC/14953-27
(OSTI ID: 758140)

DELIVERABLE 3.1.4 – INCREASED OIL PRODUCTION AND RESERVE FROM IMPROVED COMPLETION TECHNIQUES IN THE BLUEBELL FIELD, UINTA BASIN, UTAH

Topical Report
June 7, 1999

By
Milind Deo
Craig D. Morgan

Date Published: July 2000

Work Performed Under Contract No. DE-FC22-93BC14953

Utah Geological Survey
Salt Lake City, Utah

National Petroleum Technology Office
U.S. DEPARTMENT OF ENERGY
Tulsa, Oklahoma

DISCLAIMER

This report was prepared as an account of work sponsored by an agency of the United States Government. Neither the United States Government nor any agency thereof, nor any of their employees, makes any warranty, expressed or implied, or assumes any legal liability or responsibility for the accuracy, completeness, or usefulness of any information, apparatus, product, or process disclosed, or represents that its use would not infringe privately owned rights. Reference herein to any specific commercial product, process, or service by trade name, trademark, manufacturer, or otherwise does not necessarily constitute or imply its endorsement, recommendation, or favoring by the United States Government or any agency thereof. The views and opinions of authors expressed herein do not necessarily state or reflect those of the United States Government.

This report has been reproduced directly from the best available copy.

DOE/BC/14953-27
Distribution Category UC-122

Deliverable 3.1.4

Increased Oil Production and Reserves from Improved Completion Techniques in the Bluebell Field, Uinta Basin, Utah

By
Milind Deo
Craig D. Morgan

July 2000

Work Performed Under Contract No DE-FC22-92BC14952

Prepared for
U.S. Department of Energy
Assistant Secretary for Fossil Energy

Gary Walker, Project Manager
National Petroleum Technology Office
P.O. Box 3628
Tulsa, OK 74101

Prepared by
Utah Geological Survey
1594 West North Temple, Suite 3110
Salt Lake City, Utah 84114-6100

TABLE OF CONTENTS

Deliverable: Field-scale Reservoir Models

DELIVERABLE: FIELD-SCALE RESERVOIR MODELS iii

SYNOPSIS 1
BACKGROUND: FLUID FLOW THROUGH FRACTURED ROCKS 1
Explicit discrete fractures 2
Discrete fracture network (DFN) 2
Single equivalent continuum 3
Dual continuum approach 3
Naturally fractured reservoirs and their simulations 4
THE STUDY AREA 6
Geology of the area 6
Available data and study sites 9
East study area 10
West study area 12
Reservoir fluid properties 13
RESERVOIR MODELS 14
East-side four-section mode 14
West-side four-section model 15
Twenty-section models 16
Available data 17
Generation of spatial property distributions 18
Thickness distribution 18
Porosity distribution 19
Saturation distribution 20
Variation in fluids in place 20
Flow simulations 20
Reservoir models 21
Production results 21
Effect of scale on production 23
CONCLUSIONS 25
REFERENCES 26

Synopsis

Bluebell field in east-central Utah is a large, extensively fractured reservoir. Conventional dual-porosity, dual-permeability simulators were used to study production performance in parts of this reservoir. Lack of data on a number of different reservoir parameters made modeling a difficult task. The main objectives were to:

- Simulate parts of the reservoir using the conventional dual-porosity, dual-permeability approach. Generate progressively complex reservoir models and use the production history match results to quantify formation damage.
- Examine the effect of the numerical aspects such as grid sizes and fracture properties on the simulations results
- Evaluate the effect of fluid thermodynamic properties on production.
- Study effect of inclusion of fractures on variability in production from stochastically generated reservoir models.

Background: Fluid flow through fractured rocks

Various approaches have been suggested to simulate fluid flow through fractured rocks. These approaches have been applied to petroleum reservoir simulations, simulations of multiphase contaminant transport, and groundwater flow simulations. The approaches can be divided loosely into four categories (Bear, 1993).

1. Explicit discrete fracture
2. Discrete fracture network
3. Single equivalent continuum
4. Dual continuum

Above classification which is based on how the fractures are represented depends to a certain extent on scale of study. The scale starts at a few feet for explicit discrete fracture representation to thousands of feet for single equivalent continuum simulations.

Explicit discrete fractures

These models incorporate explicit, discrete representation of fractures. This approach is also been described as "very near field approach" by Bear (1993). The approach which considers flow in single fractures, consists of writing mass balance equations explicitly in individual fractures. The models allow explicit representation of fluid potential gradients and fluxes between individual fractures and between fractures and porous media. Travis (1984) and Ward et al. (1993) have developed models for explicit discrete fracture flow approach. Murphy and Thomson (1993) have solved two phase flow in a single fracture of variable aperture with the boundary element method. Other single fracture flow studies have been reported by Schrauf and Evans (1986), Tsang (1984), Tsang and Tsang (1987), Wang and Narasimhan (1985). As the number of fractures increases, the data acquisition and computational burden increase significantly. It is difficult to extend this approach to a network of fractures.

Discrete fracture network (DFN)

In this approach, the fractures are represented as a network of fractures. The flow occurs only through the fracture network and the matrix system is not considered at all. Bear (1993) calls this a "near field" approach. The individual fractures are approximated with parallel plates or planes and simplified transport equations are written for each fracture. The flow through the network is written by using mass and energy balance equations at fracture intersections. A large number of models have been developed using the discrete fracture network approach, most of which have been for applications in contaminant transport and ground water flow modeling. Rasmussen (1991) and Rasmussen and Evans (1989) have used the discrete fracture network approach and principles of the boundary element method to investigate steady state flow of water through a fractured medium. Smith and Schwartz (1984) have used two-dimensional DFN model where the flow and mass transport occur through two orthogonal fracture sets. Long et al. (1982) developed a two-dimensional DFN model where fractures were assumed to be circular disks with uniform aperture. Long et al. (1985) later extended this approach to three-dimensional computational domain. Huang and Evans (1985) have also proposed a three-dimensional

DFN approach for steady, saturated flow. A one-dimensional flow tube formulation was used to describe flow through the fracture plane.

Single equivalent continuum

This approach is also known as the "very far field approach" (Bear, 1993). When the volume of interest is large enough, the fractures and the matrix are considered to be a single equivalent continuum. This approach essentially combines the separate representation of fractures and matrix into a single medium. Various techniques are used to calculate the single set of equivalent properties for the fractured rocks. Pruess et al. (1986) developed a model for single equivalent continuum in fractured rock, where the equivalent permeability was sum of the rock and fracture permeability. Travis (1984) and Reeves et al. (1986) have proposed finite difference numerical models. Wang and Narasimhan (1985) used finite element approximations to study the fractured systems using the single equivalent approach. Brebbia and Maier (1985), Elsworth (1986, 1987), Andersson and Dverstorp (1987) applied boundary element methods with single equivalent continuum approach to solve for flow in fractured rock.

Dual continuum approach

This approach is also known as the "far field approach" (Bear, 1993). This approach was first introduced by Barenblatt et al. (1960) and later extended by Warren and Root (1963). The dual continuum approach considers the fracture and matrix as two equivalent and interacting continua. Equations of flow are written for each continuum and solved together to describe flow through fractured rock. This approach has been extremely popular in oil reservoir simulations.

Various other approaches have also been proposed for flow through fractured rocks. Bai et al. (1993) introduced a generalized multiporosity, multipermeability approach. It was shown that the dual continuum or single fracture approaches can be derived from this general approach. Pruess and Narasimhan (1982, 1985) proposed a multiple interacting continua (MINC) method. The matrix was represented as nested blocks. The fractures were on the outside of the nested matrix blocks. Since only part of the matrix interacts with the fractures during actual flow, the nested blocks are used to represent the varying

interaction between the fractures and the matrix. The innermost block has a very limited interaction with the fractures, representing parts of matrix which are not in immediate contact with the fractures. Saidi (1987) used a numerical simulator where the entire fractured reservoir was divided into a small column of matrix blocks, each representing smaller reservoirs. The fractures were used to specify the boundary conditions for each small reservoir.

The single fracture and discrete fracture network approaches are widely used in hydrology and aquifer modeling. These approaches need detailed characterization of fracture networks and are useful when the study area is small (few hundred square feet). In petroleum reservoir applications, usually the field of study is very large (several hundred acres). It is impractical if not impossible to perform detailed characterization of fracture networks for these systems. Also, implementation of these techniques will result in computationally intensive problems. The single continuum equivalent and the dual continuum approaches can be used in the field scale problems where the need for small scale variability is not that important.

Naturally fractured reservoirs and their simulations

A number of oil reservoirs in the world are naturally fractured. Some of the giant oil fields in the Middle East are fractured. These reservoirs have a wide variety of rock mineralogy. The fractured reservoirs in the middle east are mainly fractured limestones. These fields include, Ain Zalah, Kirkuk fields in Iraq, Dukhan field in Qatar, Asamari field in Iran. The Gela and Ragusa fields in Sicily are fractured dolomite reservoirs. Examples of fractured sandstone reservoirs include the Altamont-Bluebell field in Utah and the Spraberry Trend in west Texas. The Santa Maria basin in western California and La Paz-Mara field in Venezuela are examples of fractured shale reservoirs. In all of these reservoirs, the porosity and permeability of the reservoir rocks are moderate to low. Fractures provide a means of production in otherwise unproductive reservoirs. Some of the reservoirs in middle east are so extensively fractured that two to three well placed wells can drain the entire field (Van Golf-Racht, 1982).

Even though a number of fractured reservoirs exist very few numerical flow simulation studies have been reported on these reservoirs. Two studies are described below.

1. Saidi (1983) developed a numerical simulator where fractures were used to assign boundary conditions for matrix blocks. He used this simulator to simulate two fractured reservoirs in Iran, namely the Asamari formation and the Kirkuk field. Unlike the dual-porosity, dual-permeability approach, this approach did not need explicit specification of fracture properties. The fracture frequencies were characterized from core studies and flow-meter surveys. These fracture frequencies were used to determine the matrix block size. The matrix block size used was about 8 feet. The observations from limited samples were generalized over the entire reservoir. Values of a number of parameters were unavailable. These values were determined by trial and error through a production history match. This approach was used to successfully match part of the production data.
2. Thomas et al. (1987) reported results of simulations study performed on the Ekofisk reservoir. The simulations were performed with dual-porosity, dual-permeability simulators. The fractured areas were determined through comparing the well test derived permeability with rock permeability values. Blocks with effective permeability larger than the rock permeability were considered fractured and the fractures were assigned the effective permeability values. The effective permeability values were used to determine the matrix block lengths and thus fracture frequencies using following relation: $k_e = k_m + 1.69 \times 10^{10} \, b^3/L$. The fracture width, b was assumed to be 50 μm. The fracture porosity was assumed to be 0.01. The matrix block lengths were then used in the calculation of shape factors. These parameters were used to obtain a production history match. Values of various matrix and fracture properties were adjusted to obtain a satisfactory history match. The model that obtained a satisfactory history match was used to study the waterflood performance.

Above studies used various sources of information to characterize fracture properties. The fracture networks were not characterized over the entire study areas, since it will be difficult to do so. Trends in fracture properties were determined from available test results like well-test derived permeability. Approximations were made about some of the

fracture property values and their distributions. Trial and error methods were also used to obtain satisfactory history match.

There have been no field-wide flow simulations of Altamont-Bluebell field. Models were developed to study different parts of this field using the conventional modeling methods as reported by Thomas et al. (1987) and Saidi (1983).

The study area

The study area is part of the Bluebell field in eastern Utah. The Bluebell field is the largest oil producing field in the Uinta Basin. Bluebell is one of the three contiguous oil fields, Bluebell, Altamont, and Cedar Rim, shown in Figure 1. The Bluebell field is 251 square miles in size and has produced over 127 million barrels of oil and 155 billion cubic feet of associated gas so far. Most of the field is produced at a spacing of one oil well per section, though some sections have two wells.

Geology of the area

The Bluebell field produces oil from the Eocene-Paleocene Green River and Wasatch Formations near the basin center. Figure 2 shows a north-south cross-section of the Uinta Basin. The distribution of the depositional environments of the ancient lake Uinta is shown in Figure 3. Fouch (1975) has discussed different formations in the Altamont-Bluebell fields.

- North Horn Formation: The North Horn Formation includes variegated claystone, sandstone, conglomerate, and local deposits of coal and carbonate which are identified as alluvial, paludal and isolated lacustrine depositional facies.
- Flagstaff Formation: The lacustrine Flagstaff Formation lies between the fluvial beds of the North Horn and Colton Formations. The Colton Formation pinches out northward into the basin where laterally equivalent lacustrine rocks of the Green River Formation were deposited. It is difficult to distinguish between the two formations where Green River lies directly on Flagstaff. It is common practice to refer to the section as Green River Formation when Green River and Flagstaff can not be broken out, or the Flagstaff Member of the Green River Formation.
- Colton Formation: The Colton Formation lies between the Green River and Flagstaff Formations on the southwestern side of the basin. Sandstone and red claystone form

this formation. The Colton intertongues with and pinches out northward into the Green River Formation. In the southeast portion of the basin the underlying Flagstaff is absent. Where the Flagstaff is absent, the red-bed sequence below the Green River is called the Wasatch Formation. On the eastern side of the basin, the contacts between the Green River, Wasatch and North Formations are gradual and hard to define.

- Green River Formation: The Green River Formation lies on top of and interfingers with the Wasatch and Colton Formations. As can be seen from Figure 2, large portions of the Uinta Basin tertiary aged rocks are part of the Green River Formation.

The Green River and Wasatch or Colton Formations were deposited in inter-tonguing relationship. The contacts between these formations are transitional and inter-tonguing, as a result they are difficult to identify accurately. The depositional cycles indicate rapid lake level fluctuations and changes in water chemistry (Fouch, 1975). The Green River and Wasatch Formations were deposited in alluvial-fluvial, marginal lacustrine, and open lacustrine environments. The oil production in the Bluebell field comes from three primary intervals belonging to these two formations:

1. Lower Green River/ upper Wasatch transition
2. Wasatch Formation
3. Lower Wasatch transition

The Lower Green River/ upper Wasatch transition defines the transition between the top of the Wasatch Formation and the lower part of the Green River Formation, while the lower Wasatch transition defines the transition between the lower part of Wasatch and the Flagstaff Member of the Green River Formation. These three intervals are shown on a cross sectional map between two wells in the Bluebell field in Figure 4. There are a number of subsurface markers that can be identified through out the Uinta Basin. The middle marker is one of the most prominent markers identifying the top of Lower Green River.

Production from the Bluebell field was first established in the Roosevelt Unit from the Lower Green River/upper Wasatch transition at depths less than 11,000 feet. The

Productive beds in this interval are interbedded calcareous sandstone, limestone, marlstone and ostracodal limestone, deposited in fluvial-deltaic and carbonate mud-flat environments. Many of the lower Green River beds laterally extend into the Wasatch Formation. The Wasatch Formation is primarily made up of sandstone and siltstone deposited in alluvial to fluvial-deltaic environments. The source for Wasatch redbeds (sandstone, siltstone and red shale) in Bluebell field was the Uinta Mountains to the north. The Wasatch redbeds thin rapidly from north to south through the field, with the best sandstone development located in the west portion of the field. The lower Wasatch transition consists dominantly of carbonates with minor sandstone that were deposited in marginal to open lacustrine environments. The lower Wasatch is productive throughout most of the field. On the east portion of the Bluebell field, lower Wasatch is the primary productive interval, while on the west portion both the Wasatch sandstone and lower Wasatch carbonate are productive.

The oil fields in the Uinta Basin have extremely high reservoir fluid pressures (Bredehoeft et al., 1994). The average pressure gradient is around 0.5 - 0.6 psi/ft. Pressure gradients as high as 0.8 psi/ft have been reported in the central part of the field (Lucas and Drexler, 1976). The abnormally high pressures have been attributed to tight low-permeability reservoirs and local generation of hydrocarbons from kerogen within the formations due to high formation temperatures. Due to the tight nature of the reservoir rocks the fluid pressures are localized. As a result even closely spaced reservoirs have considerable pressure differential.

The Altamont-Bluebell fields are naturally fractured reservoirs (Lucas and Drexler, 1976; Narr and Currie, 1982). Because of the low permeability of the reservoir rock, oil production is dependent on the presence of natural, joint type fractures. The generation of subsurface fractures has been attributed to the regional geology, high pore-fluid pressures, temperatures, tectonic stresses and the depositional sequences (Narr and Currie, 1982). The evolution of the fracture network was gradual and formed before the generation or secondary migration of the hydrocarbons (Lucas and Drexler, 1976; Narr and Currie,

1982). Most of the fractures in the Altamont-Bluebell fields are vertical and have north-northwest orientations. The surface fracture pattern has been studied in the Bluebell field (Allison, 1987). The fracture trends follow the regional geologic structural trends. There are two dominant sets of fractures, one set has orientations north northwest while the other set is orthogonal to the first set. The fracture frequency is strongly dependent on the lithology (Lucas and Drexler, 1976). Narr and Currie also observed that the compositional and physical properties of the rocks controlled the amount of fracturing observed in a bed.

Individual beds in the lower Green River and Wasatch producing intervals are difficult to evaluate for production characteristics. Fracturing and complex formation water chemistries make conventional geophysical log analysis highly questionable. Due to the economics involved, production tests of individual beds have been discouraged. Therefore, it is not clearly understood which beds in any particular well are potentially significant producers, limited producers, water producers or thieves. As a result, the common practice is to perforate numerous beds over thousands of vertical feet and apply acid-frac treatment. A typical well in the Bluebell field has between 1,500 to 2,000 feet of gross perforations. Figure 5 shows a histogram of gross perforations in thousands of feet from a data set of 132 wells in the eastern portion of the Bluebell field. As can be seen from the figure most of the wells are perforated over thousands of feet of intervals.

Available data and study sites

The present study was concentrated in two different study areas from the Bluebell field. The reservoir rock properties were calculated from geologic logs. The following logs were available for the wells in the region:

1. Gamma Ray
2. Neutron Porosity
3. Density Porosity
4. Resistivity

The logs were available for thousands of feet of formation interval as shown in Figure 4. The geologic characterization became progressively complex in terms of number of beds identified. The logs were used to identify the middle marker and subsequently the three

productive intervals in each well. Once the productive intervals were identified, the oil-bearing beds were identified based on 60 API or less gamma ray readings (only those beds with thickness greater than 6 feet were taken into consideration). The thickness of the beds were calculated from the gamma ray readings. After the oil-bearing beds were identified, the porosity values were calculated as the average of the neutron and density porosity logs. The porosity readings were used along with the resistivity log readings in Archie's equation to calculate the fluid saturation in each bed. The porosity and saturation values represented the average values over the entire bed. Thus, the following information was available for each zone in each well.

- Thickness
- Average porosity
- Average saturation

All the identified beds were correlated through each well over the entire study area. The two study areas are described in the following sections in detail.

East study area

As the name suggests, the east study area is in the eastern portion of the Bluebell field. A 20-section area was chosen on the eastern side of the field. Figure 6 shows a map of the 20-section area and the wells in the region. This study area included the Roosevelt Unit. This area has lower Green River/upper Wasatch transition, Wasatch, and lower Wasatch transition intervals. These intervals are commingled in some of the wells. This part of the field has the poorest producers. Typically the wells from this area have produced less than 200,000 barrels of oil, some have produced even less than 100,000 barrels. Most of the sections in the Roosevelt Unit have two wells per section, while some sections have only one. As mentioned before, some of the wells in the east study area are perforated in all the three intervals over intervals spanning thousands of feet. The characterization of different beds in these intervals was performed in steps and became progressively complex. The three stages of characterizations and the different study areas are as follows.

1. A four-section area, which is part of the 20-section area was chosen for primary characterization and modeling. The four sections chosen were sections 7, 8, 17 and 18 in Township 1 South, Range 2 West. Figure 7 shows a map of the four

sections and the wells present in those sections. The area included the following wells.

a) Michelle Ute

b) A1E Ute

c) 1-18A1E

d) Chasel Sprouse

e) RU C-11

f) Malnar Pike

g) 1-17A1E Ute

The logs were used to identify five different beds in this four-section area. These beds were correlated through all the wells. The thickness, porosity and saturation values were calculated for each bed. Figure 8 shows a cross section through two of the wells, showing the five correlated beds identified as QEL1 - QEL5. All the wells with the exception of 1-17A1E are perforated in one or more of these beds.

2. Comprehensive single well models were developed for two wells in the four-section area. The two wells were Michelle Ute in section 8 and Malnar Pike in section 17. Michelle Ute is perforated in 69 different beds, while Malnar Pike is perforated in 50 different beds. The geophysical logs were used to calculate the reservoir properties for each of the perforated beds. The information included thickness of each bed, the average porosity and saturation present in each bed. A report on comprehensive single-well models has been submitted previously.

3. A detailed characterization of the entire 20-section area was performed. The logs were used to identify all the possible oil bearing beds in each well. The identified beds were correlated through all the wells in the entire 20-section area. The information on each bed included thickness, average porosity and saturation.

Side-wall core samples were available for some of the wells in the Bluebell field. Permeability values of these cores were measured by core flooding experiments (Wagner, 1996). Figure 9 shows a porosity versus permeability cross plot. The permeability data indicates extremely tight formations with very low permeability values. The fracture characterization in this area is very limited. Narr and Currie (52) reported results of

fracture analysis in the Altamont field. Utah Geological Survey has reported results of a surface fracture pattern study for parts of the Bluebell Field (Wagner, 1996). The surface fracture study was limited to orientations of fractures. No quantitative information was available in terms of subsurface or surface fracturing frequency, widths of fractures, etc. Wagner analyzed cores available from some of the wells in the Bluebell field. The results of the core analysis were reported qualitatively for fracturing densities.

West study area

The west study area is located in the western portion of the Bluebell field. Figure 10 shows the west study area and the wells in the area. The study area included sections 9, 10, 15 and 16 in Township 1 South, Range 2 West. There are seven wells drilled to the lower Green River Formation or deeper in the four sections.

1. 2-9A2 Lamicq
2. 3-10C State
3. 2-10C Springfield
4. 2-16A2 Lamb
5. 6-16A2 Boren
6. 3-15A2 Boren
7. 4-15A2 Sundance

This study area includes some of the best producing wells with cumulative production of over three million barrels of oil per well. Many of the wells were originally drilled and completed in the lower Green River/upper Wasatch transition. Oil production from this formation ranged from 93 - 436 MSTB of oil. The wells were later deepened and completed in the Wasatch Formation and lower Wasatch transition. The wells produced greater than one million barrels of oil per well. Of the above mentioned wells only Lamicq 2-9C, Springfield 2-10C and State 3-10C were perforated in the Lower Green River/ upper Wasatch transition.

The reservoir characterization for the wells in this area was performed only for the lower Green River/upper Wasatch formation. Eleven different beds were perforated in one or

more of the wells. For each of the beds, information in terms of thickness, average porosity and saturation was available. These beds were correlated through all the wells in the four-section area. Figure 11 shows a cross section of the reservoir through two of the wells in the area. Nine of the 11 correlated beds are present in these two wells. As can be seen from the figure, most of the beds have significant thickness in both the wells. The beds had cumulative thickness of 20 to 90 feet. No data on permeability of the reservoir rock were available. Similar to the east study area, quantitative information on fracture properties and their distribution was not available.

Reservoir fluid properties

Oil and gas samples from two of the wells in the region were collected. Experiments were performed to measure the oil API gravity, oil viscosity and thermodynamic properties. The details of the experiments and the results were provided in earlier annual reports. The gas specific gravity was 0.75. The geologic and fluid property information was used to develop a number of different models for parts of Bluebell field. The API gravity of two oils from the wells in the Roosevelt unit were 31.5 and 32 respectively. Glasso (1980) has derived empirical relationship between the bubble point pressure and dissolved gas as a function of oil API gravity, gas specific gravity and temperature. The relationship was derived from experimental measurements of properties of a number of gas and oil samples from the North Sea reservoirs. These empirical relations were used to calculate the pressure versus dissolved gas relationship. The gas gravity of 0.75 was used. The oil API gravity was varied from 22 API to 32 API. The reservoir temperature was varied between 200 to 250 °F. Figures 12 a and b show the variation of pressure and oil formation volume factor with dissolved gas for three oil API gravity values. As the API gravity increases the gas solubility increases. On the other hand, changes in API gravity do not have a significant impact on the oil formation volume factor. As shown in Figures 13 a and b, varying the temperature from 200 to 250 °F does not have a significant impact on either the pressure or oil formation volume factor at a particular solution gas volume. These thermodynamic properties and bulk properties were used to develop reservoir models and to study their effect on production behavior of a fractured reservoir model.

Reservoir models

The numerical models developed were fractured models based on the conventional dual-porosity, dual-permeability approach. In this approach, the fractures are treated like a continuum similar to the nonfractured rock (also known as the matrix). For every grid block the fractures are characterized in terms of the properties such as porosity, permeability, frequency, etc.

- Fracture frequency: The fracture frequency denotes the number of fractures per unit length. The fractures are assumed to be orthogonal and present in the principle coordinate directions. The fracture frequency determines, to a large extent, the amounts of fluids transferred between the matrix and fractures.
- Fracture porosity: Fracture porosity is defined as the fraction of the reservoir volume occupied by fractures. The fracture porosity is equivalent to the matrix porosity. The changes in rock fracturing can be taken into account by specifying spatially varying fracture porosity.
- Permeability of fractures.

In addition to these properties, fluid saturations, initial pressure, initial bubble point pressure, and relative permeability-saturation curves are also required for fractures. Assumptions were made about the numerical values of fracture properties due to the lack of quantitative information. Various numerical models are described below.

The four-section models

The east-side four-section model was a preliminary model, since it took into account only some of the beds responsible for production. On the other hand, the west-side model was developed for all the beds that were responsible for the production.

East-side four-section model

The numerical parameters used for various properties are listed in Table 1. The reservoir extended from 13000 to 14000 feet. The model had 20 grid blocks in the x and y directions. The x and y dimensions of the grid blocks were 528 feet each. Low porosity and low permeability layers separated the five correlated zones, which resulted in nine blocks in the vertical direction. The reservoir rock porosity varied between 0.0 and 0.18.

The initial reservoir pressure varied with the depth at a gradient of 0.5 psi/foot. The initial GOR was 900 scf/stb at a initial bubble point pressure of 4146 psi. The initial oil saturation was constant at 0.7.

The thickness, porosity and saturation data were calculated from the well logs and thus represented properties at the well bore. The values observed at well bore were assumed continuous over the area surrounding the wells. The values of matrix permeability and fracture properties were obtained through field production history match. The values used for these properties are listed in Table 1. Limited fracturing was assumed. Only about a million square feet area surrounding each of the wells was assumed fractured. The fractures were vertical and present only in the x and y directions. The fracture frequency was 1 fracture per 10,000 feet. The fracture porosity was constant at 0.05 % of the reservoir volume.

Figures 14a and b compare the model predictions for cumulative oil and gas production for the entire four-section area with the field data. The production performance for Michelle Ute well is compared in Figures 15a and b. As seen from the figures, the model does a good job of matching the cumulative oil production. For the four-section area, the gas production predictions are higher than the field data, while for the Michelle Ute well, the gas production prediction lags the field data. The final pressure distributions for the model are plotted in Figure 16 along with the individual well locations. As can be seen from the figure, except for the Chasel Sprouse and RU C11 wells, the drainage radius of wells does not extend over to the next well. The history match was obtained with very low values for matrix permeability as well as fracture properties. The values used for matrix permeability were in the range of 0.018 - 0.33 mD. The values of fracture porosity, permeability and frequency were also very low.

West-side four-section model

Information in terms of bed thickness, average porosity and saturation were calculated from the logs. Similar to the east-side model, the reservoir properties were available at the

well locations. The property values were assumed to be continuous over the area surrounding the wells. The parameters used to develop the model are listed in Table 2.

The vertical extent of the reservoir was from 10,250 to 10628 feet. The entire four square mile area was divided on a grid with 20 blocks in x and y directions each. The x and y dimensions of the grid blocks were 528 feet each. The 11 oil bearing zones were separated by low-porosity and low-permeability zones, which resulted in 21 layers. The vertical dimensions of the grid blocks varied according to the individual bed thickness. The matrix porosity varied between 0 % and 26 %. The initial oil saturation varied between 0.7 and 0.9. Similar to the east-side model, the pressure varied at a gradient of 0.5 psi/foot. The initial GOR was 400 scf/stb and the initial bubble point pressure was 2100 psi. Field production history match was obtained by adjusting the values of rock permeability and fracture properties. The values that obtained the final production match are tabulated in Table 2.

Figures 17a and b show the comparison between the model predictions and the field data for cumulative oil and gas production for the four-section area. The production predictions for well 3-10C State are compared with the field production data in Figures 18a and b. As seen from the figures, the model does a good job of matching the final field production data.

Twenty-section models

Stochastic simulations are widely used to generate reservoir property distributions. These property distributions can be used to assess the reservoir production variability. This section discusses the effect of inclusions of fractures on the production variability. A 20-section area was chosen on the eastern side of the Bluebell Field. The details of the study area were described earlier.

The geophysical logs were used for detailed characterization of most of the beds present in the 20-section area on the eastern side of the Bluebell field. Most of the oil-bearing beds were identified and correlated through out the 20-section area. The characterization led to information in terms of thickness, porosity and saturation for all the beds. No

information on rock types or lithotypes distributions was available. Principles of geostatistics were used to generate property distributions from the available data. Reservoir models were developed to study the effect of stochastic distribution of properties on fluid production.

Available data

The general geology of this region was presented earlier in the report. The oil bearing zones are part of three different intervals; lower Green River/upper Wasatch transition, Wasatch and lower Wasatch transition. Most of the wells in this region are perforated in at least one of these intervals. The middle marker is a major geologic marker that can be correlated throughout the 20-section area. The middle marker identifies the top of the lower Green River/ upper Wasatch formation.

The oil-bearing beds were identified based on Gamma Ray readings of 60 API or less and 6% porosity. Once the beds that met the above criterion were identified in each well, they were correlated through all the other wells in the 20-sections area. Some of the beds did not have property values above the cutoff threshold in all the wells. These beds were still considered in model development. In all, 85 different beds were identified over the entire 20-section area. However, none of the wells had all the 85 beds present.

The two comprehensive single well models discussed earlier were developed using only the perforated beds. Michelle Ute well was perforated in 69 different beds, but for this study 77 different beds were identified in Michelle Ute. Some of the perforated beds did not qualify for present analysis due to their failure to meet the cutoff criterion. Limited information on matrix permeability values was available and no information on fracture properties was available. The reservoir characterization resulted in the following information for 20-section area:

- Correlated beds in different wells
- Thickness of beds in each well
- Average porosity in each bed
- Average saturation in each bed

The information about various property values was available at the well locations. In order to develop reservoir models, property distributions in the 20-section area were necessary. For the four section area models and the single well models, the property values observed at the well bore locations were assumed continuous through out the model area. For this study, the available data were used to generate stochastic spatial distributions of reservoir properties over the 20-section area.

Generation of spatial property distributions

The conventional methods used to develop reservoir models using stochastic techniques are described in geostatistical text books. The specific methods used in this study are presented in detail elsewhere (Pawar, 1998). In order to use those methods, information on rock type distributions, sands distributions within individual rock types and porosity-permeability distributions is required. For the present study such information was not available. Due to lack of the data, the reservoir models were not generated for all the beds. Instead the stochastic distributions of properties for different beds were obtained individually and independent of other beds. Stochastic simulations were performed using the principles of sequential Gaussian simulations. In order to perform the stochastic simulations, the parameters for spatial variability were calculated for each property in each zone. The calculation of spatial variability and subsequent simulations were performed with normally transformed data sets.

Thickness distribution

The spatial variability was calculated in terms of two-dimensional thickness variograms. Principle directions of continuity and anisotropy factors were determined by comparing a number of semivariograms in multiple directions. Figure 19 shows a semivariogram of thickness for bed 30. The thickness data in this zone did not show any principle direction of continuity hence an omni-directional semivariogram was chosen. The semivariogram did not show any structural anisotropy. The semivariogram was calculated at a minimum lag spacing of 220 feet. Figure 19 also shows a model fit to the semivariogram. The model was an exponential model. The model had no nugget effect. The semivariogram had a range of 3000 feet. A sill of 1.0 was used, since the semivariogram was calculated

for a normal data set. The semivariograms for thickness of all the zones were calculated in similar fashion. The model parameters for thickness semivariograms for all the beds are compiled in Pawar (1998).

The structure of the semivariograms for different beds was similar. All of the semivariograms were omni-directional. Different beds in parts of the 20-section area different beds might have exhibited local anisotropy, but when the entire 20-section area was considered, none of the semivariograms showed a principle direction of continuity. Some of the beds had higher correlation lengths than others. Since all of the semivariograms were calculated for the normally transformed data sets a sill of 1.0 was used.

The spatial variability information was used to generate multiple thickness realizations. These realizations were conditioned to the observed thickness values at the well locations. The output of stochastic simulations was transformed back to the original data format (from normal distributions). Figure 20 shows one realization for thickness distribution in bed 30. Multiple thickness distributions were generated for all the beds.

Porosity distribution

The distributions of porosity were also generated in two dimensions for each bed. two-dimensional semivariograms were calculated to determine measures of continuity. Figure 21 shows an omni-directional variogram for porosity in bed 30. The omni-directional semivariogram was chosen due to lack of structural anisotropy calculated through number of different directional semivariograms. The semivariogram was calculated at a lag spacing of 220 feet. Figure 21 also shows the model fit to the semivariogram. The model had one exponential structure. The correlation range was 1320 feet. There was no nugget effect and the sill was 1.0. The semivariogram structures were similar to the thickness semivariograms. Multiple, conditional realizations of porosity distributions were generated using the semivariogram model. Figure 22 shows a realization of porosity in bed 30.

Saturation distribution

The spatial distributions of saturation data were generated using similar steps. A semivariogram for saturation in bed 30 is shown in Figure 23. Figure 23 also shows the model fit to the semivariogram. The model had an exponential component with a range of 1320 feet. The nugget effect was 0.0 and the sill was 1.0. Multiple conditional realizations of saturations were generated with the spatial variability parameters. The realizations were conditioned to the observed saturation data. Figure 24 shows one such realization for saturation distribution in bed 30 through the 20-section area. Similar distributions were generated for all the beds. The stochastic realizations of various properties were generated for all the beds independent of one another.

Variation in fluids in place

The information on thickness, porosity and saturation was used to generate models for different beds. These models were used to study variations in fluids in place. Four different realizations of porosity, thickness and saturations were generated for each of the beds. The resulting property distributions were combined to generate 64 different models for each bed.

Some of the beds have high average OOIP compared to others. Most of the beds have average OOIP of the order of 1-8 million STB. These beds are not continuous over a large part of the 20-section area. Thickness realizations for four beds are compared in Figure 25. The four beds are 18, 25, 30, and 38a. Beds 25 and 38a have low average OOIP, 5.75 MSTB and 5.0 MSTB respectively. As can be seen from the figure, these beds have zero thickness over most of the 20-sections area. On the other hand, beds 18 (42.5 MSTB) and 30 (37.2 MSTB) have high average OOIP due to thicker oil bearing zones over the domain, as can be seen from Figure 25.

Flow simulations

The stochastically generated data sets were used to develop reservoir models. Due to the large number of beds and limitations of flow simulator, it was impossible to take all the beds into account. In order to study the flow performance, independent and separate

reservoir models were developed for different beds. Six different, reasonably continuous beds were chosen. All the chosen beds had high average OOIP. The six beds were 13, 18, 19, 23, 30 and 31.

A number of different reservoir models were developed from multiple property data sets. Flow simulations were performed with these models to study the effect of fractures on production variability. Flow simulations were performed on ten different reservoir models for each bed. The 10 models considered were chosen randomly from the 64 models used for OOIP studies.

Reservoir models

The flow simulations were performed with both fractured as well as nonfractured models. The fractured models were conventional dual-porosity, dual-permeability models. The numerical values for different parameters are tabulated in Table 3. The models had 41 and 33 blocks in the x and y directions. The x and y dimensions of each block were 660 feet. There was only one block in the vertical direction. The thickness of the grid blocks varied according to the stochastically generated thickness values. The porosity and saturation of the matrix also varied according to geostatistically generated data. The permeability of the matrix was assumed to be constant at 0.5 mD. The fracture porosity was assumed to be 0.005. The fracture frequency was 1 per 220 feet. The permeability of the fractures was assumed to be 1.5 mD. The fracture properties were assumed to be continuous over the entire 20-section model. The reservoir fluid and thermodynamic properties were similar to the earlier models. The variations in the production performance of these models are discussed below.

Production results

The flow simulations were performed over a period of 8 years. All of the wells were open during this period of time. The statistics of the production results for both fractured and nonfractured reservoir models for each zone are summarized in Table 4. Production from

the entire 20-section area, and Michelle Ute and Malnar Pike wells are compared in the table.

As can be seen from the table the presence of fractures makes a big difference in the amount of oil produced. The production in bed 18 tripled due to the presence of fractures; however, the gas production increased six times. The GOR for the fractured model thus increased from 945 scf/stb to 1660 scf/stb. GOR values of about 1000 scf/stb are more common in the field than values around 1500 scf/stb. The Michelle Ute and the Malnar Pike wells appeared to be affected differently due to the presence of fractures. The production in Michelle Ute increased by an order of magnitude while the production from Malnar Pike only doubled. Since the fracture representation is uniform around both the wells, the production is related to other reservoir characteristics around the wells, such as bed thickness, porosity and saturation. Production responses from beds 19 and 23 are similar to the trends observed for bed 18. Oil production from these beds for the fractured model increases two to four times while the gas production increase is six to eight times. Thus the effective GOR values for the fractured model are 1.5-3 times higher than the nonfractured models. Once again, the production from Michelle Ute increases significantly more than the production from Malnar Pike. The water saturation for Michelle Ute in zone 23 is 100%. In a nonfractured environment, there is no avenue for the drainage of oil that lies beyond the well grid block. The fractures provide this drainage capability and as a result the oil production in Michelle Ute for bed 23 goes up almost two orders of magnitude. Fractures provide a much larger drainage radius and the fact that Michelle Ute is the only well in its section (section 7) obviously contributes to the observed enhancement in production. The quality of the reservoir around each of the wells also plays an important role.

Beds 30 and 31 also show the same trends with respect to overall oil and gas productions (for the 20-section area). However, the increase in oil and gas productions for the Michelle Ute and Malnar Pike wells is comparable for these two beds. The standard deviation in both the oil and gas production is significantly lower in the fractured model

compared to the nonfractured model. Thus, introduction of a uniform fracture network reduces production uncertainties resulting due to the use of equally probable reservoir images of the nonfractured rock mass. In the dual-porosity dual-permeability approach the fractures act as the main pathways for production. The matrix rock acts only as a source of oil to the fractures. Once the fractures are introduced, they dominate production and reduce the importance of a more accurate representation of the matrix. Even with low values of fracture property parameters, the production from the fractured models for these six zones is much greater than the actual field production. This points to the following possibilities.

- Most of the fractures are closed and for all practical purposes, the reservoir behaves as if it is nonfractured.
- There are even fewer fractures than are represented in the fractured models.
- There is an extensive formation damage at the well bore preventing the realization of the full production potential of each well.

These results are similar to the results for the four-section area models and the single well models. The sensitivity of these models to following fracture properties were studied (Pawar, 1998).

- Fracture frequency
- Fracture porosity
- Fracture permeability

The results were similar to the single well model results, details of which were provided in an earlier report.

Effect of scale on production

It was observed that the low values for different fracture parameters result in low drainage radius for the wells. The reservoir models described earlier were used to study the effect of scale of representation. The single well models for Michelle Ute and Malnar Pike wells were described in a previous report. The effect of scale was studied by using reservoir models for one bed.

In the twenty section models, the production was studied for six different beds. Of the six beds both Michelle Ute and Malnar Pike wells are perforated only in bed 18. The reservoir models for this bed were used to compare the production performance of the single well models and the 20-section area models. The values of fracture properties and matrix permeability used for the 20-section area models were different from the values used for single well models. In the present study, the values of these properties were the same as the ones used for single well models. Limited fracturing was assumed for the area surrounding the well block. Values of fracture porosity, permeability and frequency were listed in Table 3. All the other properties like initial pressure, bubble point pressure, thermodynamic and rock-fluid properties were also the same as the single well models. Flow simulations were performed for 10 different models.

The production results for this bed are compared in Table 5. The table compares the average of cumulative oil and gas production from the layer for Michelle Ute and Malnar Pike wells for the single well model and 20-section model. The total oil production for the Michelle Ute well is about 100,000 stb, while the gas production is about 90 MM scf. For the Malnar Pike well the total oil production is about 84,000 stb, while the gas production is about 80 MM scf. As can be seen from the table for Malnar Pike model there is not a significant difference between the two predictions. For this well the matrix permeability values used were extremely low (0.0001 mD), hence the production is not very significant for both the models. For the Michelle Ute well the oil and gas production are significantly different. The matrix permeability values used for Michelle Ute well were 0.14 mD. For the single well model only a 40-acre area surrounding the well was considered for production. The pressures around this well for the two cases are compared in Figure 26. As can be seen from the pressures for the single well model, the average pressure is much lower than the 20-section model. Due to the surrounding high pressure blocks the production for Michelle Ute well for the 20-section model is more. The average pressure for the 20-section model is still above the bubble point pressure. Thus, for this layer the scale has an effect on production for Michelle Ute well but not for Malnar Pike well.

Conclusions

The production performance of parts of the naturally fractured reservoirs in the Bluebell field was studied through flow simulations performed on numerical models. Two models were developed for Four Sections areas on the east and the west portions of the field. The east-side model was a preliminary model as it took into account only some of the zones responsible for production. The west-side model was developed for the zones responsible for production at the time. Two comprehensive models were developed for two wells on the east portion of the field. These models took into account all the perforated zones. All the models were developed based on the information available through geophysical log analysis. Lack of data on some of the required parameters made model development a challenging task. The numerical values of these parameters were obtained through production history match. Extremely low values of matrix rock permeability and fracture properties were needed for matching production history. The low values of the rock permeabilities are in agreement with the observed values. On the other hand, low values of fracture properties suggest that either the fractures are not contributing to the flow or the field operations have resulted in extensive formation damage near the well bore rendering in noncontributing fractures. The amount of formation damage was quantified through time dependent permeabilities of well bore blocks. A 20-section area on the east side of the Bluebell Field was used to study the effect of fracture on production variability from stochastically generated data. The available geophysical logs were used to identify and characterize all the oil-bearing zones in the entire 20-section area. Reservoir rock properties were calculated for all the zones based on properties calculated from log analyses. Stochastic simulations were performed to generate distributions of rock properties. These simulations were then used to study the variability in fluids in place. A number of zones in the 20-section area had significant amounts of fluids in place. Most of the zones in the 20-section area were not continuous over the entire area. Inclusion of fractures reduced the variability in the production from the 20-section area. In the dual-porosity, dual-permeability approach, the fractures are the main pathways for the flow while the matrix acts as source of fluids. Only the matrix properties were generated through stochastic simulations and the fracture properties were continuous over the study area. Since the fractures dominated the flow, the variability in production due to matrix

properties was reduced. Effect of various fracture properties on the production behavior of the fractured reservoir was also studied. As fracture porosity increased, oil and gas production also increased due to increased oil in place in fractures. Increasing the fracture permeability increased the oil production up to a certain value of permeability, but beyond that the production was limited by the rate of fluid transfer between matrix and fractures. Increase in fracture frequency also increased the oil and gas production only up to a certain fracture frequency. Beyond that particular frequency, the increase in fracture frequency had only a marginal effect on production. Effect of variation in fluid thermodynamic properties on the production was also studied. Increasing the oil API gravity resulted in increased oil production and reduced gas production. Increasing the reservoir temperature did not have any effect on the production performance.

The effect of scale was studied on the production for two wells in the reservoir. The study was performed only for one layer. The results showed that the production performance of Michelle Ute well was affected by scale of study. The production for single well model where only a 40-acre area around the well was studied was lower than the production for 20-section area. The continuity of the sand around the well did increase the production significantly even with low values of fracture and matrix flow properties.

References

Allison, M., 1995: "Increased Oil Production and Reserves from Improved Completion Techniques in the Bluebell Field, Uinta Basin, Utah," Annual Report, USDOE Contract No. DE-FC22-92BC14953 (1995) 1-38.

Andersson, J. and Dverstorp, B., 1987: "Conditional Simulations of Fluid Flow in Three-Dimensional Networks of Discrete Fractures," *Water Resources Research* (Oct. 1987) 1876-1886.

Bai, M., Elsworth, D. and Roegiers, J. C., 1993: "Multiporosity/Multipermeability approach to the Simulation of Naturally Fractured Reservoirs," *Water Resources Research* (June 1993) 1621-1633.

Barenblatt, G. I., Zheltov, I. P., and Kochina, I. N., 1960: "Basic Concepts in the Theory of Seepage of Homogeneous Liquids in Fissured Rocks," J. *Applied Mathematics* (USSR), (1960) **24**, No. 5, 1286-1303.

Bear, J., 1993: "Flow and Contaminant Transport in Fractured Rock," ed. Bear, J., Tsang, C., and de Marsily, G., Academic Press Inc., CA (1993) 1-40.

Brebbia, C. A. and Maier, G. (Eds.), 1985: "Boundary Elements VII - Volume 2, Proceedings of the 7th International Conference," Villa Olmo, Loake Como, Italy, Springer-Verlag (1985) .

Bredehoeft, J. D., Wesley, J. B. and Fouch, T. D., 1994: "Simulations of the Origin of Fluid Pressure, Fracture Generation, and the Movement of Fluids in the Uinta Basin, Utah," *AAPG Bulletin* (Nov. 1994) 1729-1747.

Elsworth, D., 1986: "A Model to Evaluate the Transient Hydraulic Response of Three-Dimensional Sparsely Fractured Rock Masses," *Water Resources Research* (Dec. 1986) 1809-1819.

Elsworth, D., 1987: "A Boundary Element-Finite Element Procedure for Porous and Fractured Media Flow," *Water Resources Research* (Apr. 1987) 551-560.

Fouch, T. D., 1975: "Lithofacies and Related Hydrocarbon Accumulations in Tertiary Strata of the Western and Central Uinta Basin, Utah," in Bolyard, D. W. ed., Symposium on deep drilling frontiers in the central Rocky Mountains: Rocky Mountain Association of Geologists Special Publications (1975) 163-173.

Glasso, O., 1980: "Generalized Pressure-Volume-Temperature Correlations," *JPT* (May 1980) 785-795.

Huang, C. and Evans, D. D., 1985: "A 3-Dimensional Computer Model to Simulate Fluid Flow and Contaminant Transport Through a Rock Fracture System," Report NUREG/CR-4042, U. S. Nuclear Regulatory Commission, (1985) 100-108.

Long, J. C. S., Remer, J. S., Wilson, C. R. and Witherspoon, P. A., 1982: "Porous Media Equivalents for Networks of Discontinuous Fractures," *Water Resources Research* (June 1982) 645-658.

Long, J. C. S., Gilmour, P., Witherspoon, P. A., 1985: "A Model for Steady Fluid Flow in Random Three-Dimensional Networks of Disc-Shaped Fractures," *Water Resources Research* (Aug. 1985) 1105-1115.

Lucas, P. T. and Drexler, J. M., 1976: "Altamont-Bluebell- A Major Naturally Fractured Stratigraphic Trap," *AAPG Memoir* (1976) **24**, 121-135.

Murphy, J. R. and Thomson, N. R., 1993: "Two-Phase Flow in a Variable Aperture Fracture," *Water Resources Research* (Oct. 1993) 3453-3476.

Narr, W. and Currie, J. B., 1982: "Origin of Fracture Porosity-Example from Altamont Field, Utah," *AAPG Bulletin* (Sep. 1982) 1231-1247.

Pawar, R. J., 1998: "Reservoir Characterization and Reservoir Simulation of Fractured and Nonfractured Systems", Ph.D. Dissertation, (1998), University of Utah, Salt Lake City, UT.

Pruess, K. and Narasimhan, T. N., 1982: "On Fluid Reserves and the Production of Superheated Steam from Fracture, Vapor-Dominated Geothermal Reservoirs," *Journal of Geophysical Research* (Nov. 1982) **87**, No. B11, 9329-9339.

Pruess, K. and Narasimhan, T. N., 1985: "A Practical Method for Modeling Fluid and Heat Flow in Fractured Porous media," *SPEJ* (Feb. 1985) 14-26.

Pruess, K., Wang, J. S. Y. and Tsang, Y. W., 1986: "Effective Continuum Approximation for Modeling Fluid Flow in Fractured Porous Tuff," Report SAN F86-7000, Sandia National Laboratories (1986) 1-60.

Rasmussen, T. C., 1991: "Steady Fluid-Flow and Travel-Times in Partially Saturated Fractures Using a Discrete Air-Water Interface," *Water Resources Research* (Jan. 1991) 67-76.

Rasmussen, T. C. and Evans, D. D., 1989: "Fluid Flow and Solute Transport Modeling Through Three-Dimensional Networks of Variably Saturated Discrete Fractures," Report NUREG/CR-5239, (1989) 1-15.

Reeves, M., Ward, D. S., Johns, N. D. and Cranwell, R. M., 1986: "Theory and Implementation for SWIFT II," Report NUREG/CR-3328, U.S. Nuclear Regulatory Commission, (1986) 185-189.

Saidi, A. M., 1983: "Simulation of Naturally Fractured Reservoirs," paper SPE 12270 presented at the SPE Symposium on Reservoir Simulation, San Francisco (1983).

Saidi, A. M., 1987: "Reservoir Engineering of Fractured Reservoirs," Total Edition Presse, Paris (1987) 35-105.

Schrauf, T. W. and Evans, D. D., 1986: "Laboratory Studies of Gas Flow Through a Single Natural Fracture," *Water Resources Research* (May 1986) 1253-1265.

Smith, L. and Schawrtz, F. W., 1984: "An Analysis of the Influence of Fracture Geometry on Mass Transport in Fractured Media," *Water Resources Research* (Sep. 1984) 1241-1252.

Thomas, L. K., Dixon, T. N., Evans, C. E., and Vienot, M. E., 1987: "Ekofisk waterflood Pilot," *JPT* (Feb. 1987) 221-232.

Travis, B. J., 1984: "TRACR3D: A Model of Flow and Transport in Porous/Fractured Media," LA-9667-MS, Los Alamos National Laboratory, Los Alamos, NM (May 1984) 1-35.

Tsang, Y. W., 1984: "The Effect of Tortuosity on Fluid Flow Through a Single Fracture," *Water Resources Research* (Sep. 1984) 1209-1215.

Tsang, Y. W. and Tsang, C. F.,1987: "Channel Model of Flow Through Fractured Media," *Water Resources Research* (Mar. 1987) 467-479.

Van Golf-Racht, T. D., 1982: "Fundamentals of Fractured Reservoir Engineering," Elsevier, Amsterdam (1982) 1-215.

Wagner, M.: "Core Analysis and Description as an Aid to Hydrocarbon Production Enhancement: Lower Green River and Wasatch Formation, Bluebell Field, Uinta Basin, Utah," M. S. Thesis, Brigham Young University (1996).

Wang, J. S. Y. and Narasimhan, T. N., 1985: "Hydrologic Mechanism Governing Fluid Flow in a Partially Saturated, Fractured, Porous Medium," *Water Resources Research* (Dec. 1985) 1861-1874.

Ward, D. S., Harrover, A. L. and Vincent, A. H., 1993: "Data Input Guide for SWIFT/486, Release 2.53", GeoTrans, Inc., Sterling, VA (1993) 1-60.

Warren, J. E., and Root, P. J., 1963: "The Behavior of Naturally Fractured Reservoirs," *SPEJ* (Sep. 1963) 245-255.

Table 1: Parameters for east-side four-section model.

Parameter	Value
Reservoir extent	13000 - 14000 feet
Grid	20 * 20 * 9
Grid block size (x and y)	528 feet
Porosity	0.0 - 0.18
Permeability	0.018 - 0.33 mD
Fracture frequency	1 per 10000 feet
Fracture porosity	0.0005
Fracture permeability	0.023 - 0.04 mD
Pressure	0.5 psi / foot
Oil gravity	35 API
Gas gravity	0.75
Initial GOR	900 scf/stb
Initial bubble point pressure	4146 psi
Initial oil saturation	0.7
Bottom hole pressure	3000 psi

Table 2: Parameters used for the west-side four-section model.

Parameter	Value
Reservoir extent	10250-10628 feet
Grid	20 * 20 * 21
Grid block size (x and y)	528 feet
Porosity	0.0 - 0.26
Permeability	0.08 - 0.18
Fracture porosity	0.0005
Fracture frequency	1/5000 feet
Fracture permeability	0.07 - 0.1
Pressure	0.5 psi / foot
Oil gravity	35 API
Gas gravity	0.75
Initial GOR	400 scf/stb
Initial bubble point pressure	2100 psi
Initial oil saturation	0.7 - 0.9
Bottom hole pressure	2500 psi

Table 3: Numerical parameters for the 20-section models.

Parameter	Value
Grid	41* 33 * 1
Grid block size (x and y)	660 feet
Matrix Permeability	0.5 mD
Pressure	0.5 psi / foot
Oil gravity	35 API
Gas gravity	0.75
Initial GOR	900 scf/stb
Initial bubble point pressure	3950 psi
Initial oil saturation	0.7 - 0.9
Bottom hole pressure	2500 psi

Table 4: Statistics of production from 20-section area for five beds.

Bed 18 (nonfractured)

Statistics	20-section area			Michelle Ute			Malnar Pike		
	Oil (MSTB)	Gas (MMSCF)	Water (MSTB)	Oil (MSTB)	Gas (MMSCF)	Water (MSTB)	Oil (MSTB)	Gas (MMSCF)	Water (MSTB)
Average	785.38	742.24	42.45	20.48	16.73	11.92	35.33	36.84	0.06
Minimum	681.07	680.40	41.06	18.48	11.72	10.84	13.58	19.56	0.0
Maximum	897.95	809.67	43.66	22.44	19.07	18.10	49.33	44.65	0.21
Standard deviation	60.83	37.58	0.86	1.35	2.11	2.20	12.47	8.99	0.08

Bed 18 (fractured)

Statistics	20-section area			Michelle Ute			Malnar Pike		
	Oil (MSTB)	Gas (MMSCF)	Water (MSTB)	Oil (MSTB)	Gas (MMSCF)	Water (MSTB)	Oil (MSTB)	Gas (MMSCF)	Water (MSTB)
Average	247.40	4228.20	19.41	231.06	260.57	7.43	89.95	136.82	0.001
Minimum	2321.70	3925.60	16.30	194.21	242.04	6.53	64.06	89.60	0.00
Maximum	2994.50	4497.60	23.23	263.25	289.00	8.98	132.56	173.24	0.009
Standard deviation	136.40	150.07	1.42	21.53	11.98	0.51	20.09	22.37	0.002

Table 4 continued.

Bed 19 (nonfractured)

Statistics	20-section area			Michelle Ute			Malnar Pike		
	Oil (MSTB)	Gas (MMSCF)	Water (MSTB)	Oil (MSTB)	Gas (MMSCF)	Water (MSTB)	Oil (MSTB)	Gas (MMSCF)	Water (MSTB)
Average	967.11	898.94	39.44	96.25	80.27	7.41	29.11	26.66	0.88
Minimum	894.44	874.15	38.58	82.98	70.49	7.11	17.34	16.51	0.62
Maximum	1003.00	912.60	40.65	110.01	90.88	7.67	38.23	33.29	1.02
Standard deviation	31.65	13.38	0.66	8.66	6.43	0.18	7.17	5.43	0.13

Bed 19 (fractured)

Statistics	20-section area			Michelle Ute			Malnar Pike		
	Oil (MSTB)	Gas (MMSCF)	Water (MSTB)	Oil (MSTB)	Gas (MMSCF)	Water (MSTB)	Oil (MSTB)	Gas (MMSCF)	Water (MSTB)
Average	2850.31	5401.70	12.92	345.31	508.86	3.00	78.19	152.18	0.15
Minimum	2699.40	5123.20	11.18	315.56	469.93	2.60	59.72	99.90	0.00
Maximum	3043.70	5756.10	14.81	373.11	553.13	3.43	105.93	191.22	0.35
Standard deviation	101.13	173.15	0.89	16.42	14.70	0.29	14.04	24.77	0.11

Table 4 continued.

Bed 23 (nonfractured)

Statistics	20-section area			Michelle Ute			Malnar Pike		
	Oil (MSTB)	Gas (MMSCF)	Water (MSTB)	Oil (MSTB)	Gas (MMSCF)	Water (MSTB)	Oil (MSTB)	Gas (MMSCF)	Water (MSTB)
Average	993.23	846.47	274.84	1.71	1.51	73.01	18.24	15.31	8.27
Minimum	681.36	754.64	221.01	0.00	0.00	0.00	11.81	9.91	4.87
Maximum	1106.70	944.67	349.62	8.55	7.49	129.63	31.99	26.50	11.86
Standard deviation	77.28	65.16	35.28	3.44	3.05	46.87	6.85	5.61	2.32

Bed 23 (fractured)

Statistics	20-section area			Michelle Ute			Malnar Pike		
	Oil (MSTB)	Gas (MMSCF)	Water (MSTB)	Oil (MSTB)	Gas (MMSCF)	Water (MSTB)	Oil (MSTB)	Gas (MMSCF)	Water (MSTB)
Average	4441.68	8156.44	179.04	161.28	215.33	44.85	132.76	228.94	7.94
Minimum	4228.90	7689.00	121.23	146.39	197.75	18.97	108.92	200.45	2.15
Maximum	4799.4	8508.5	279	185.17	237.91	63.7	171.71	280.4	14.73
Standard deviation	140.99	172.50	42.91	9.62	9.47	15.71	19.09	18.96	3.98

Table 4 continued.

Bed 30 (nonfractured)

Statistics	20-section area			Michelle Ute			Malnar Pike		
	Oil (MSTB)	Gas (MMSCF)	Water (MSTB)	Oil (MSTB)	Gas (MMSCF)	Water (MSTB)	Oil (MSTB)	Gas (MMSCF)	Water (MSTB)
Average	431.80	370.78	268.57	21.73	18.45	29.96	15.71	13.25	22.97
Minimum	351.28	301.11	217.24	12.41	10.55	23.58	7.58	6.37	19.99
Maximum	496.39	422.1	374.22	28.29	24.05	42.06	27.79	23.59	26.45
Standard deviation	46.85	39.99	47.77	6.13	5.20	6.12	6.66	5.68	2.14

Bed 30 (fractured)

Statistics	20-section area			Michelle Ute			Malnar Pike		
	Oil (MSTB)	Gas (MMSCF)	Water (MSTB)	Oil (MSTB)	Gas (MMSCF)	Water (MSTB)	Oil (MSTB)	Gas (MMSCF)	Water (MSTB)
Average	3492.84	6255.07	214.93	340.49	505.51	31.34	235.06	432.78	22.93
Minimum	3142	5771	146.97	305.1	446.66	15.9	186.72	361.05	15.48
Maximum	3819.2	6710	312.66	377.43	576.28	52.19	313.14	519.57	32.91
Standard deviation	202.35	243.60	41.60	16.52	26.82	9.22	35.28	38.74	4.45

Table 4 continued

Bed 31 (nonfractured)

Statistics	20-section area			Michelle Ute			Malnar Pike		
	Oil (MSTB)	Gas (MMSCF)	Water (MSTB)	Oil (MSTB)	Gas (MMSCF)	Water (MSTB)	Oil (MSTB)	Gas (MMSCF)	Water (MSTB)
Average	298.07	256.42	263.89	28.43	24.16	22.08	36.67	29.40	20.77
Minimum	243.00	212.91	223.4	17.89	15.21	15.58	23.96	19.07	16.24
Maximum	370.97	314.43	330.56	43.91	37.32	31.70	62.51	51.64	27.66
Standard deviation	48.39	38.03	30.72	8.65	7.35	5.51	12.96	11.21	4.69

Bed 31 (fractured)

Statistics	20-section area			Michelle Ute			Malnar Pike		
	Oil (MSTB)	Gas (MMSCF)	Water (MSTB)	Oil (MSTB)	Gas (MMSCF)	Water (MSTB)	Oil (MSTB)	Gas (MMSCF)	Water (MSTB)
Average	2824.33	4720.75	208.43	342.69	425.56	24.51	324.28	576.83	19.06
Minimum	2546.1	4346.9	126.38	309.51	388.35	12.35	276.58	494.88	13.28
Maximum	3222.2	5090.3	324.02	372.2	473.41	33.94	425.48	691.76	27.98
Standard deviation	192.73	183.56	41.43	18.33	22.28	7.0	39.21	45.58	3.57

Table 5: Comparison of production for two model scales.

Michelle Ute				Malnar Pike			
20 Section model		Single well model		20 Section model		Single well model	
Oil (MSTB)	Gas(MSCF)	Oil (MSTB)	Gas(MSCF)	Oil (MSTB)	Gas(MSCF)	Oil (MSTB)	Gas(MSCF)
9.607	8.400	6.896	6.900	0.080	0.060	0.050	0.045

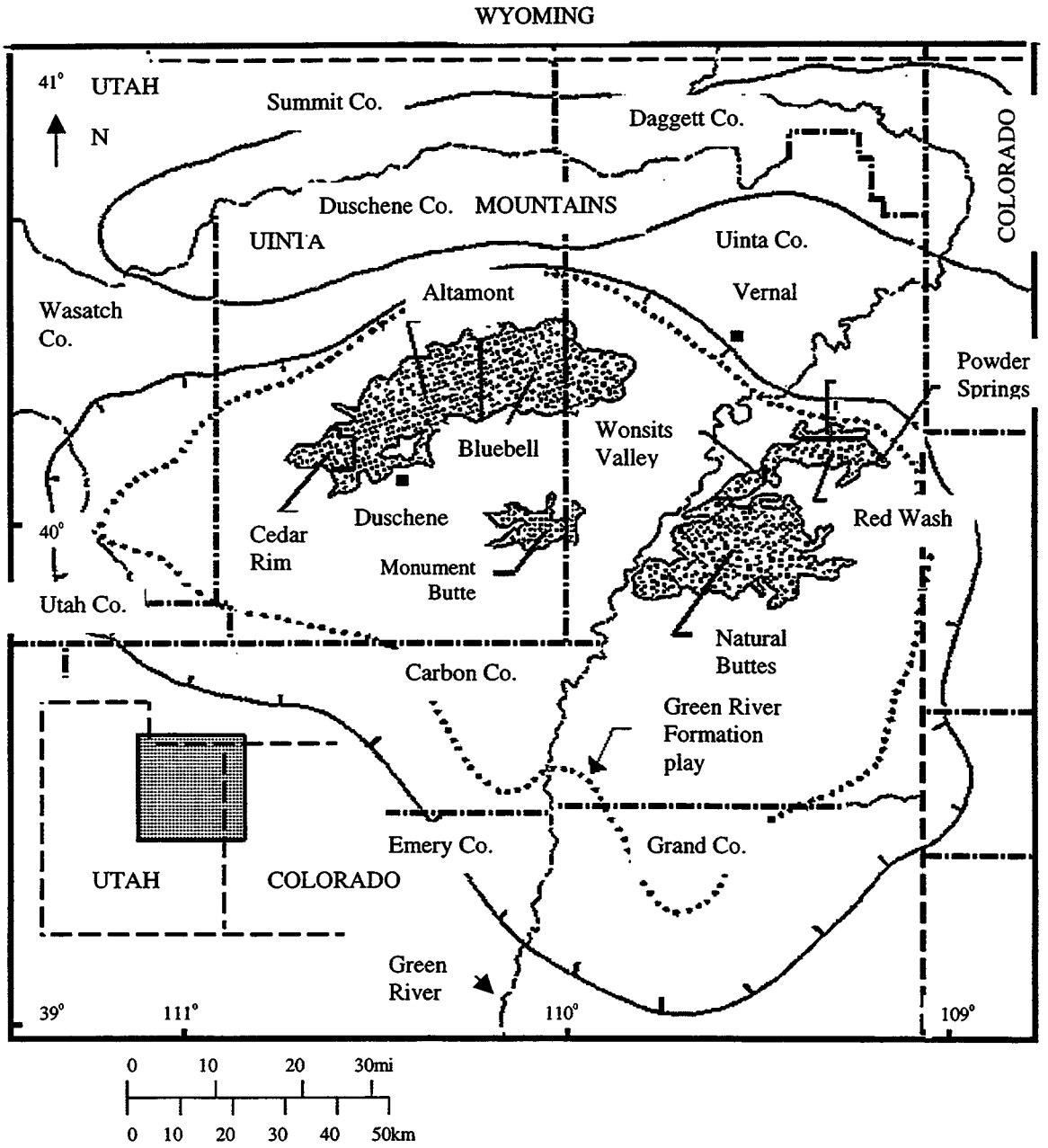

Figure 1: A map of the oil fields in Uinta Basin (Allison, 1995).

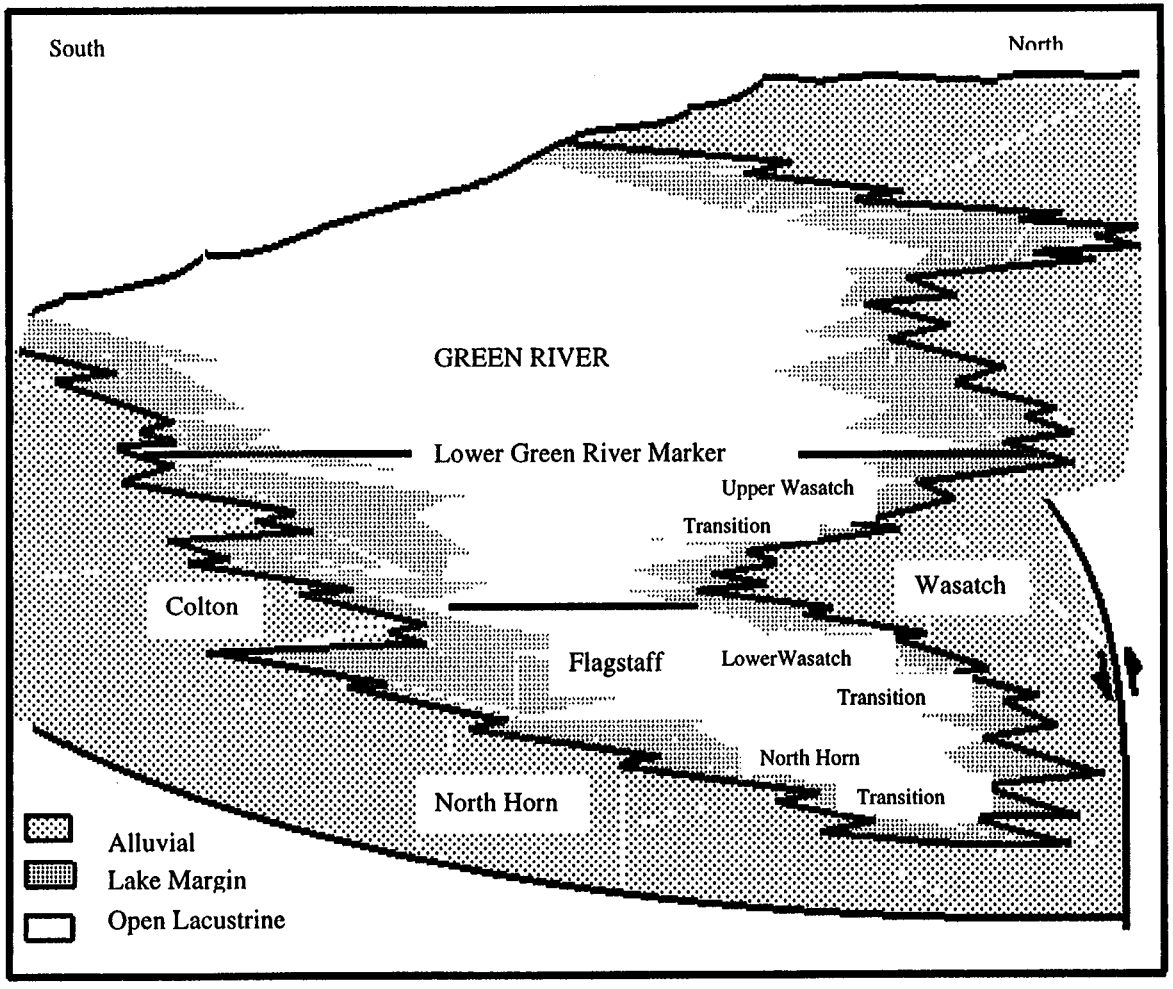

Figure 2: A north-south cross section through Uinta Basin.

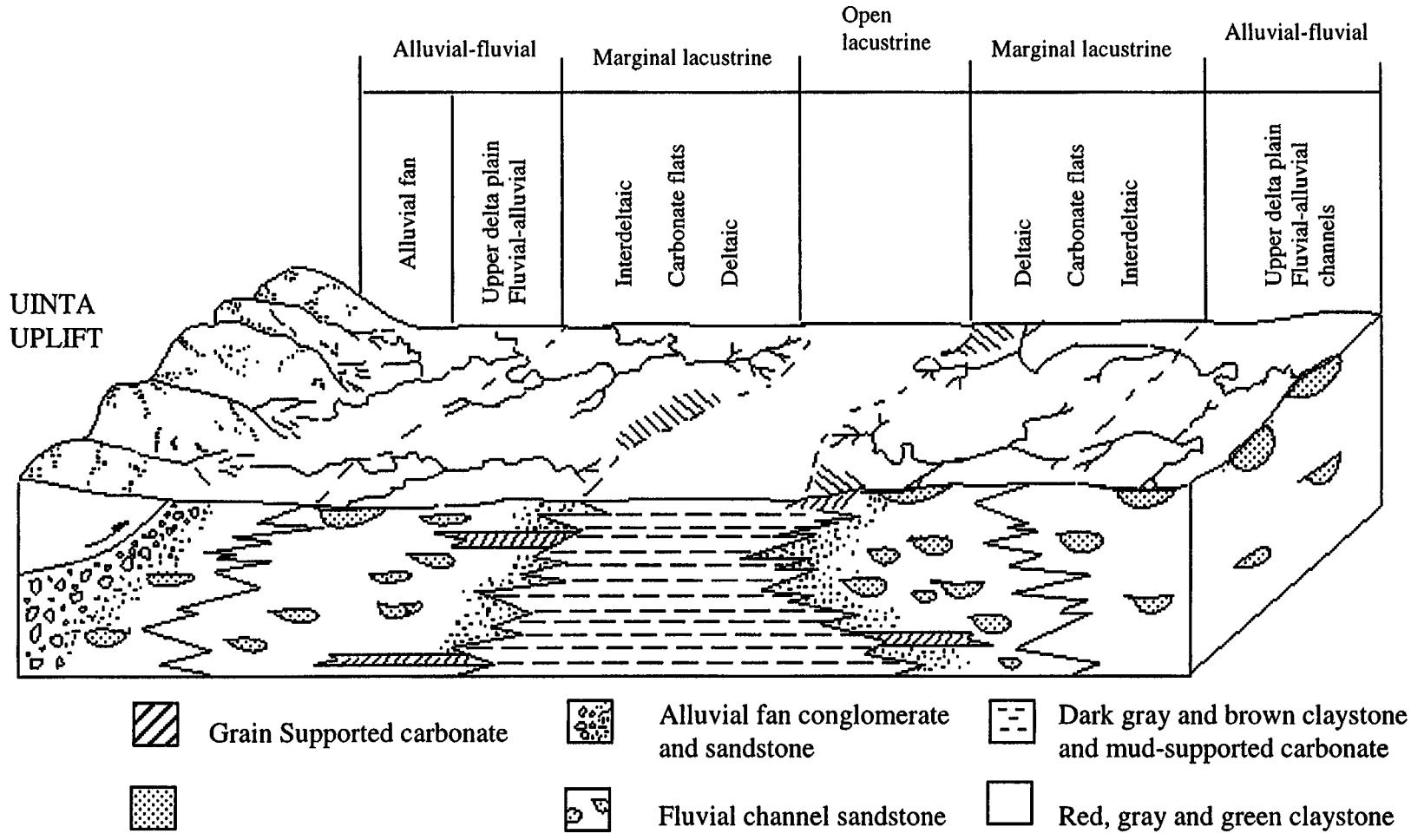

Figure 3: A Conceptual diagram of various depositional environments in the Uinta Basin (Allison, 1995).

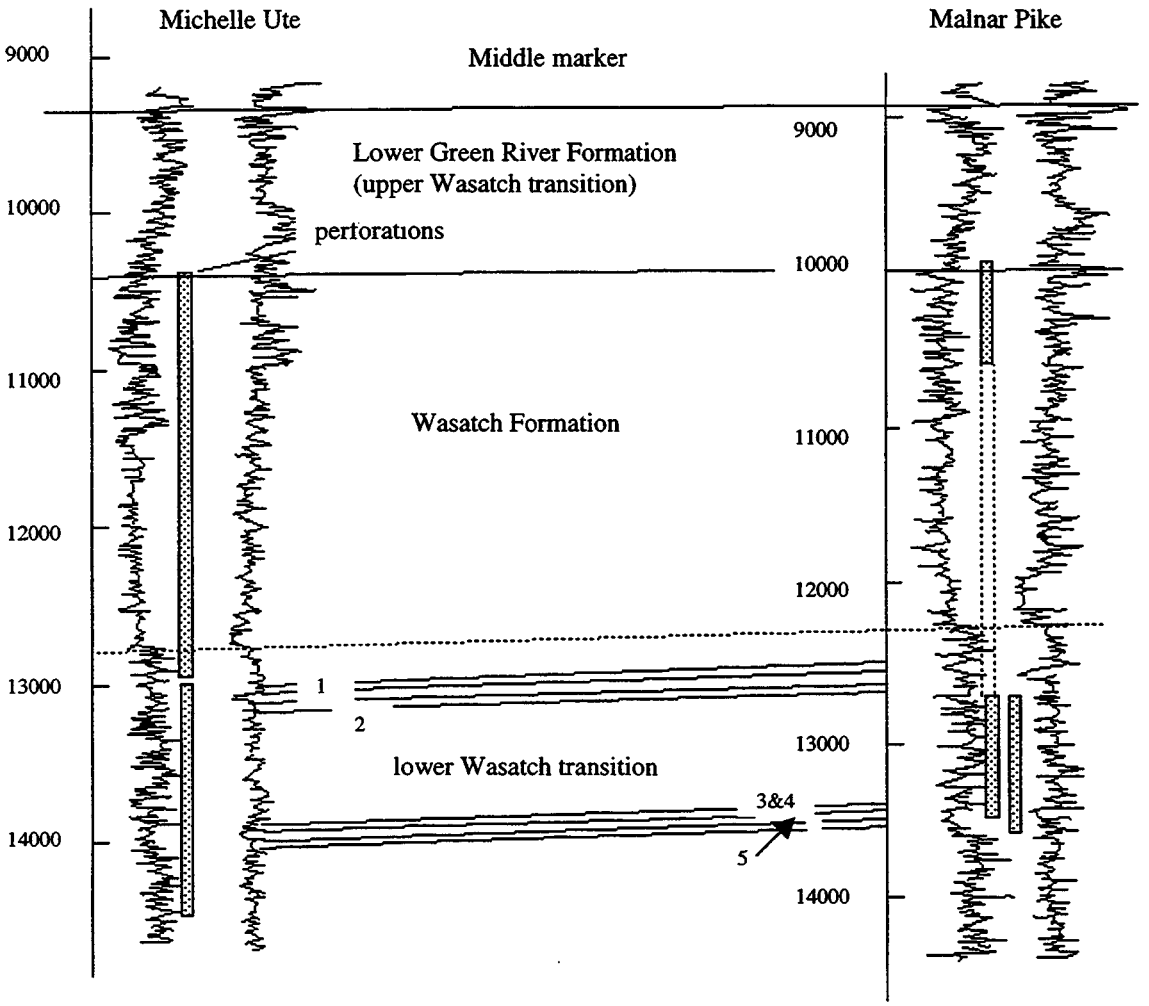

Figure 4: A cross-sectional map showing three intervals in the Bluebell field (reproduced from Allison, 1995).

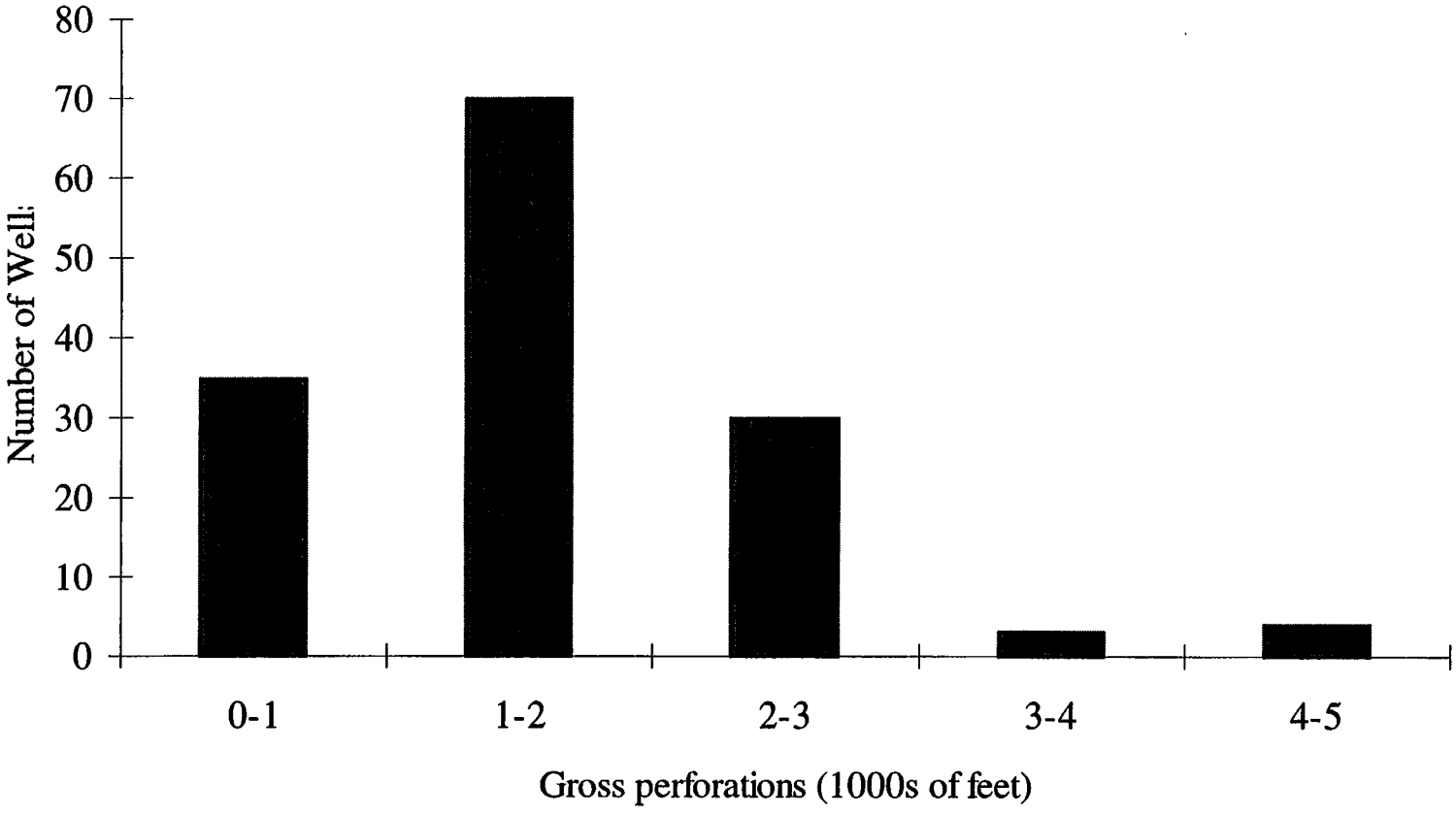

Figure 5: A histogram of gross perforations in the eastern portion of the Bluebell field.

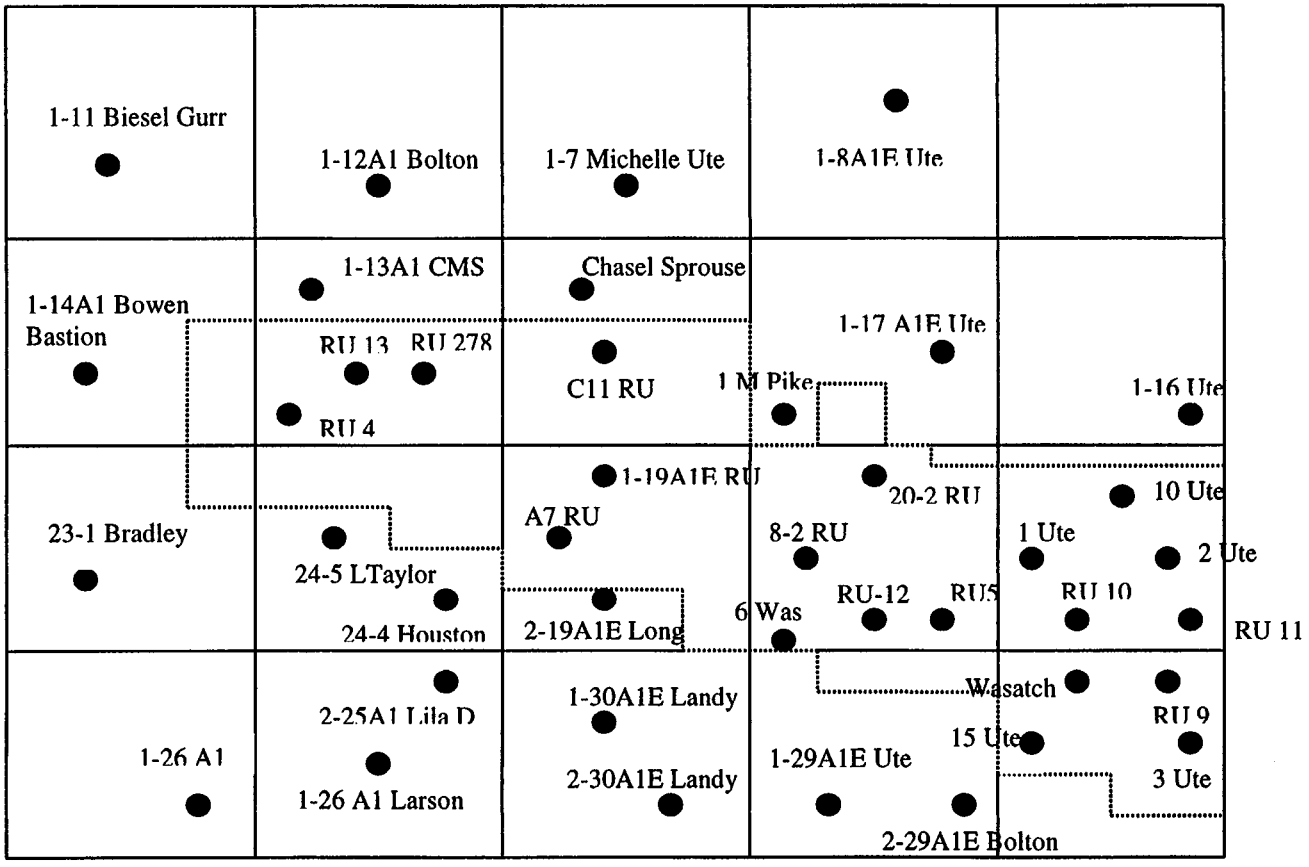

Figure 6: A map of the 20-section study area on the east-side of the Bluebell field.

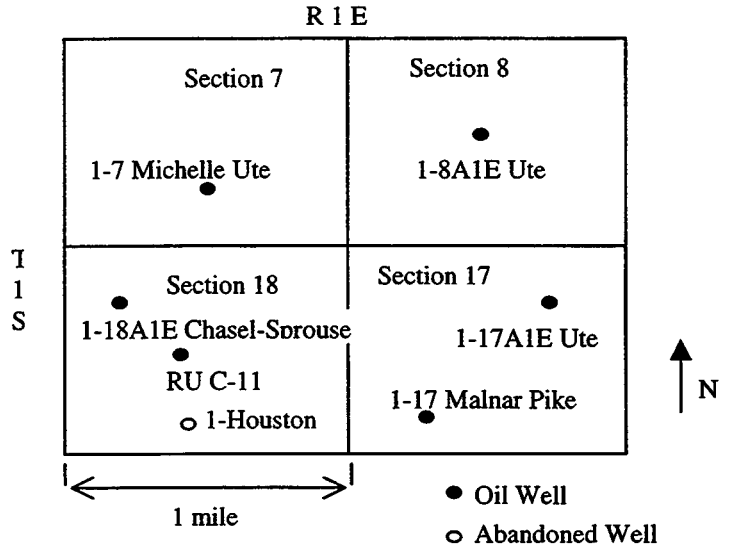

Figure 7: A map of the four-section area on the east-side of the Bluebell field.

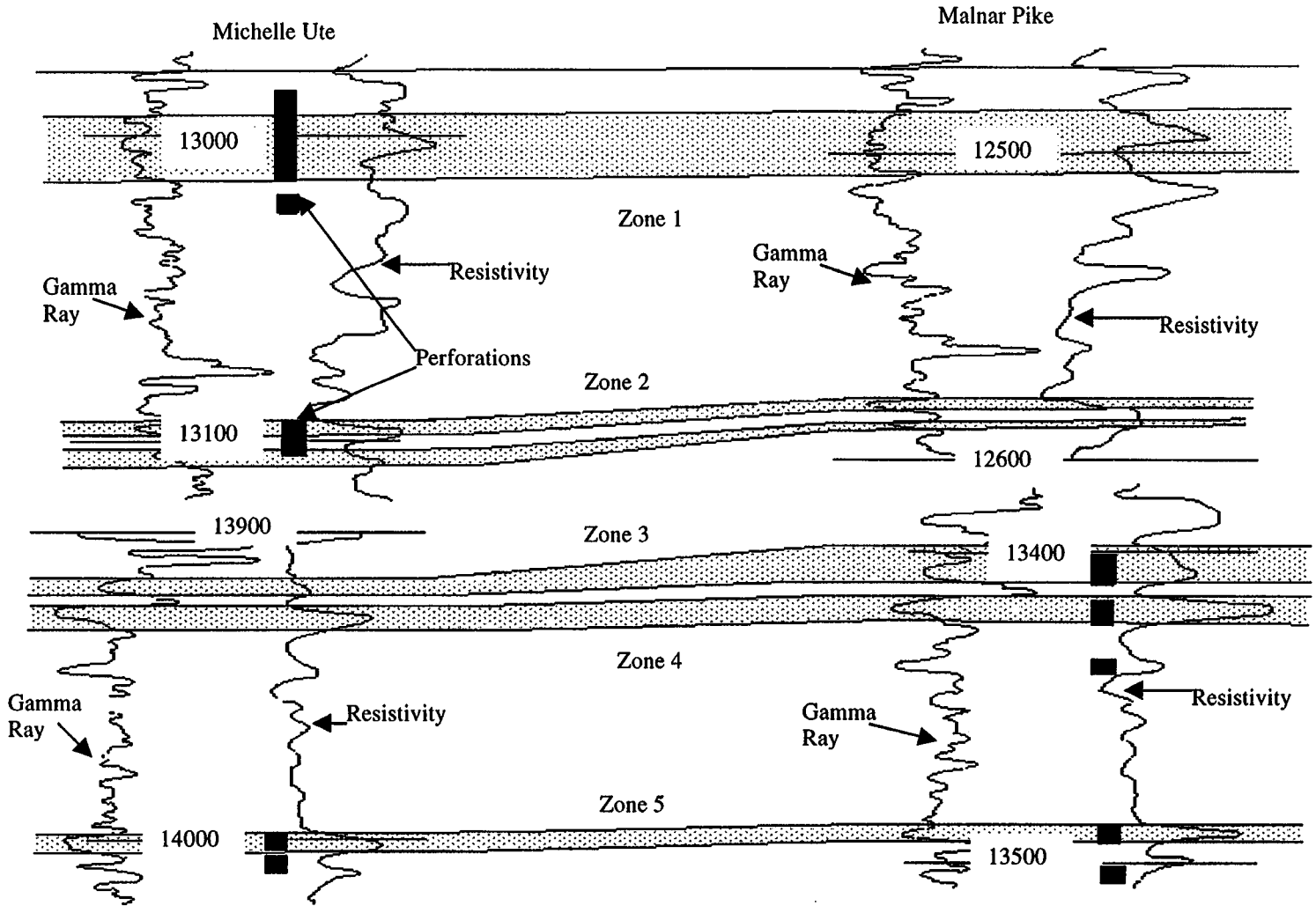

Figure 8: A cross section of the east-side four sections showing the five correlated zones (Allison, 1995).

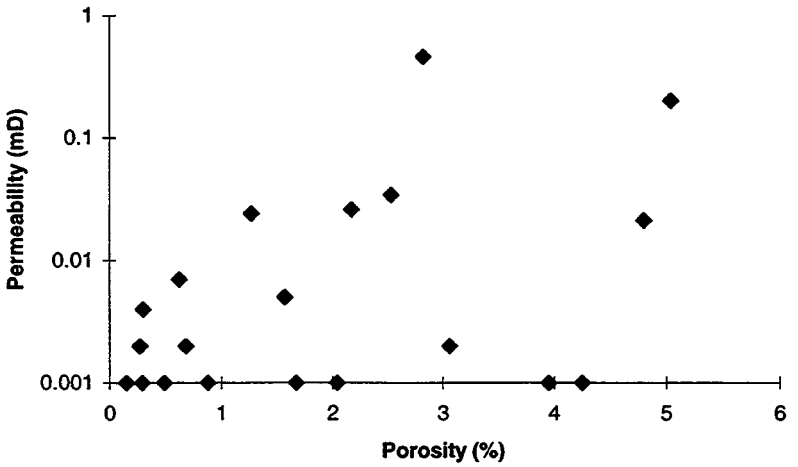

Figure 9: A porosity versus permeability cross plot for core plugs from the Bluebell field.

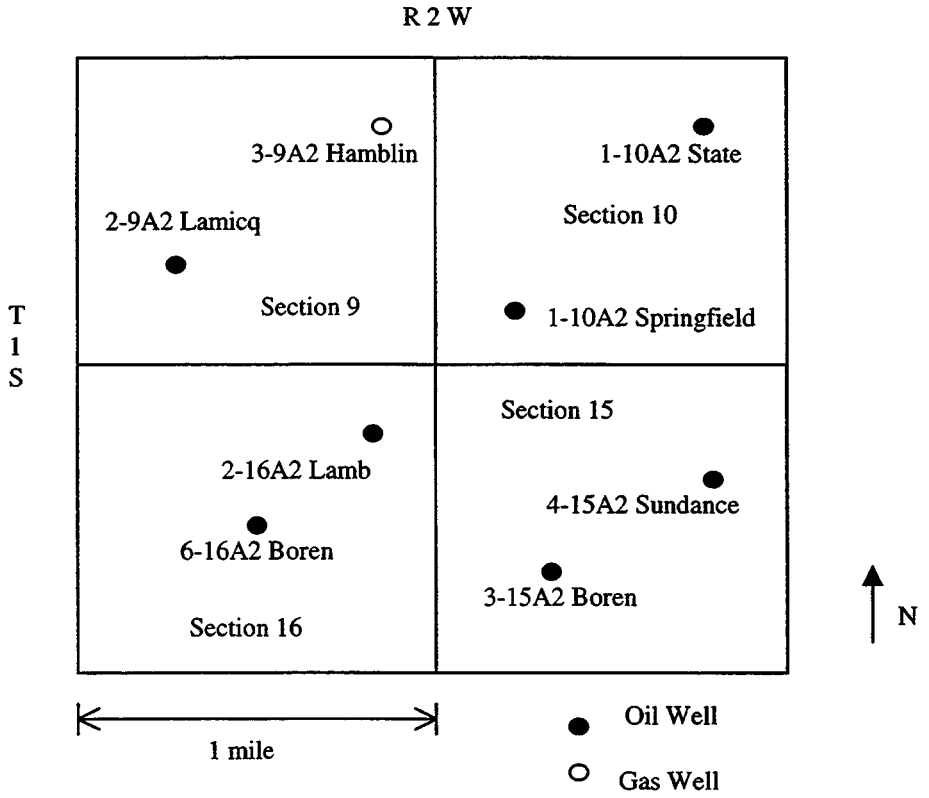

Figure 10: A map of the four-section area on the west-side of the Bluebell field.

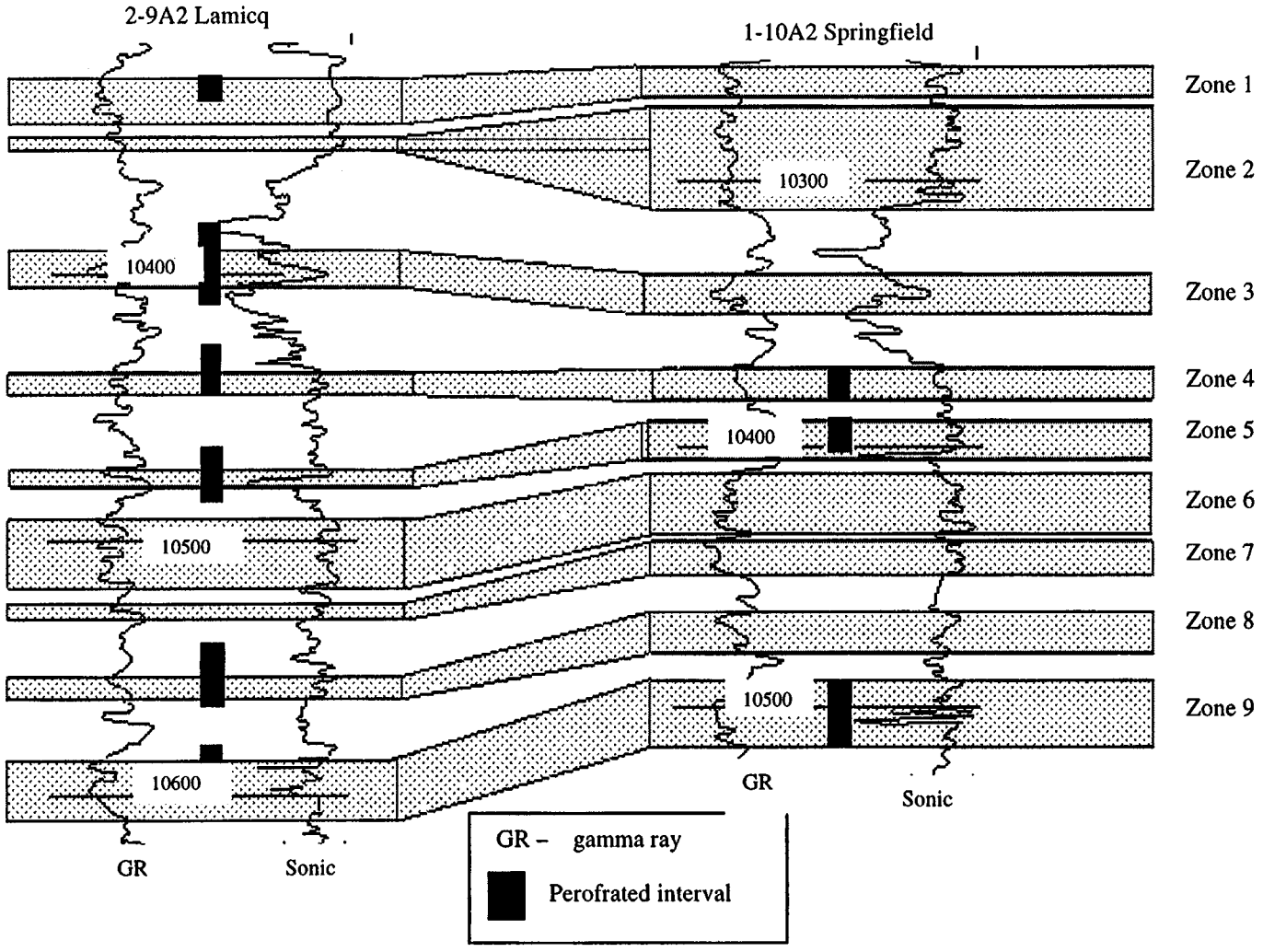

Figure 11: A cross section of the west-side four sections showing 9 of 11 correlated beds (Allison, 1995).

a)

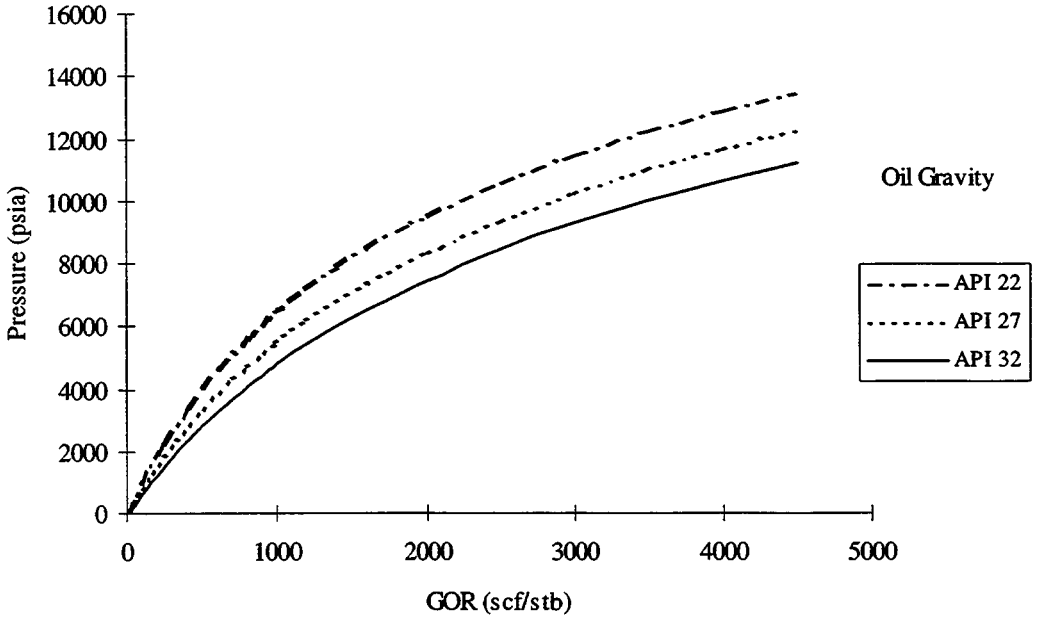

b)

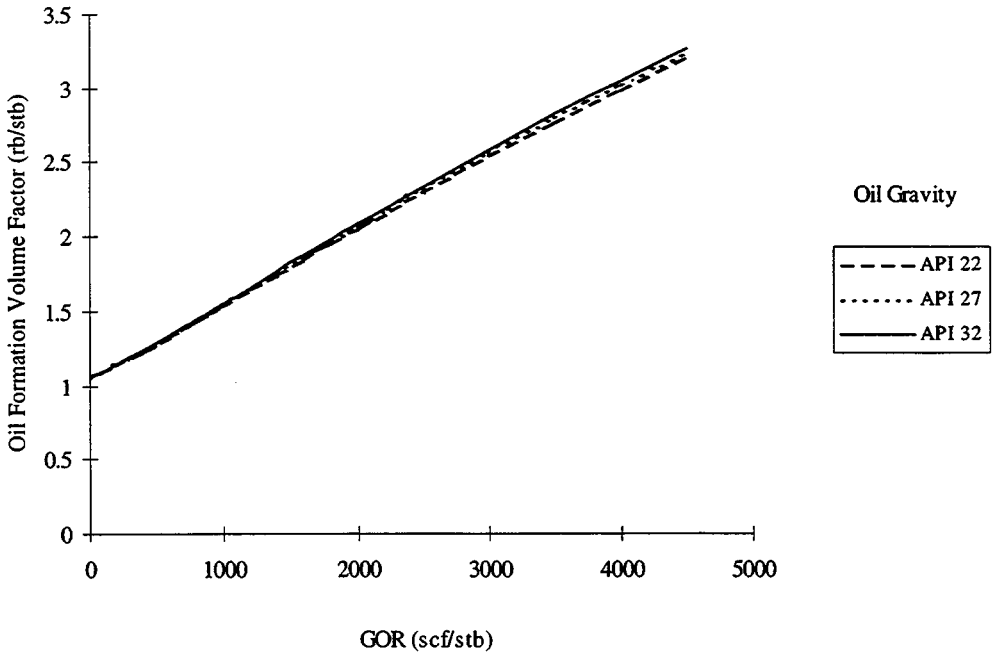

Figure 12: Effect of API gravity on thermodynamic properties at 240 °F: a) bubble point pressure versus GOR, b) oil formation volume factor versus GOR.

a)

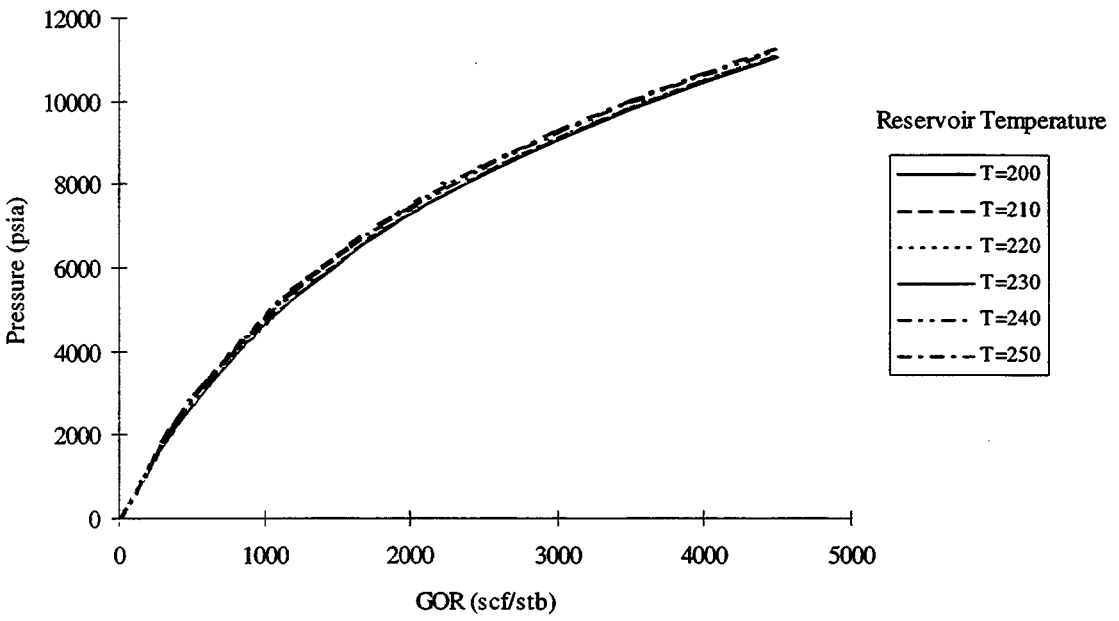

b)

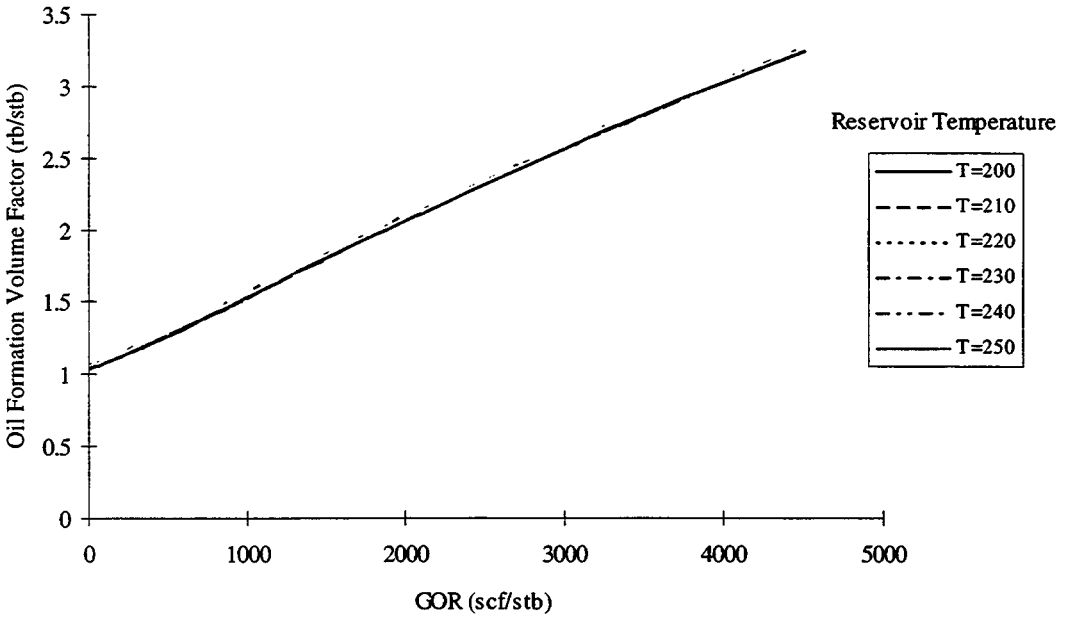

Figure 13: Effect of temperature on thermodynamic properties for 32 API oil and 0.75 gas gravity: a) bubble point pressure versus GOR, b) oil formation volume factor versus GOR.

a)

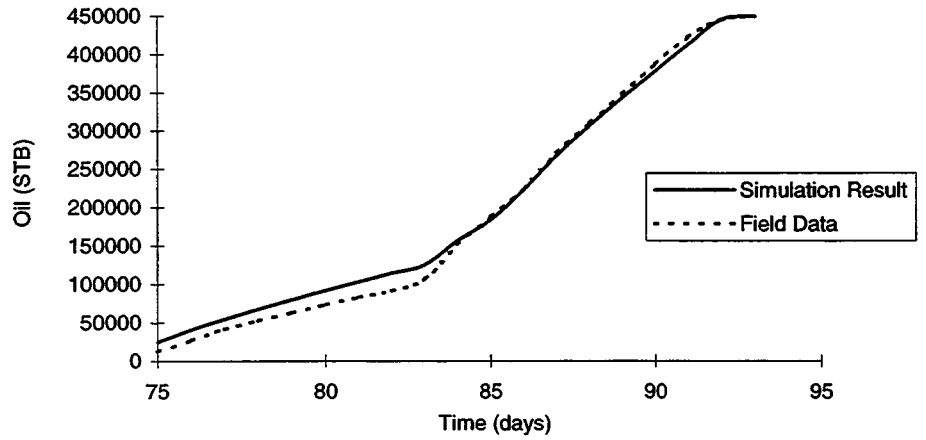

b)

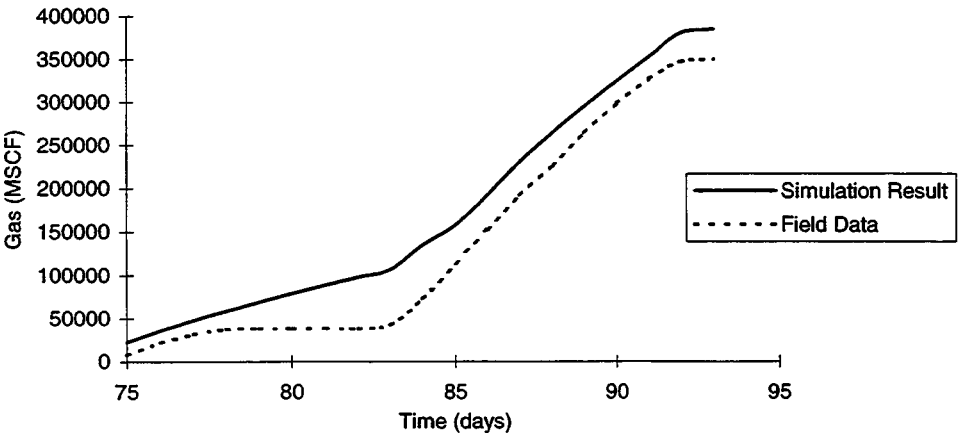

Figure 14: Comparison of the field production data to the simulation results for the east-side four-section area: a) cumulative oil production, b) cumulative gas production.

a)

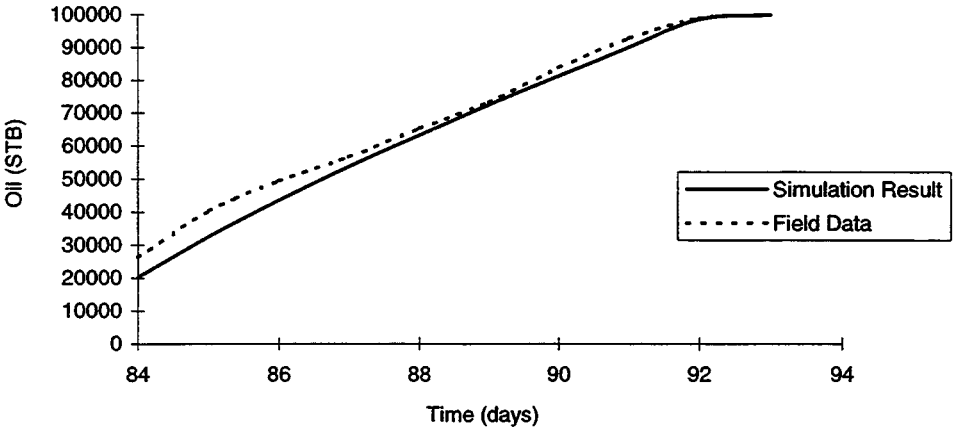

b)

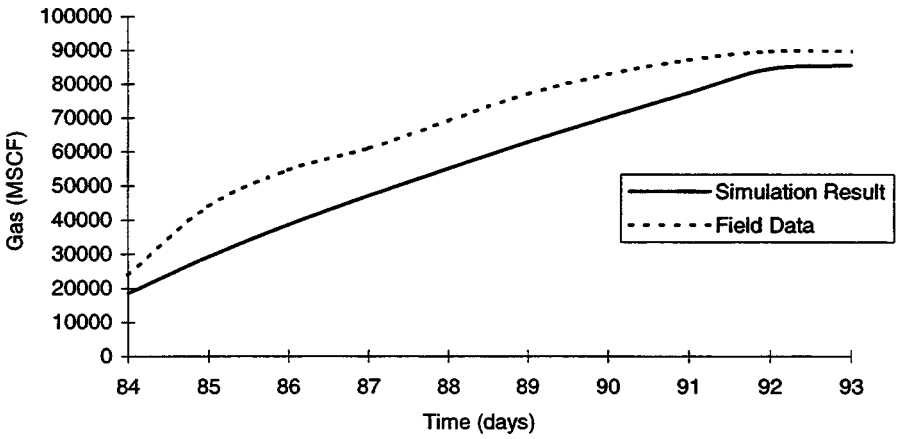

Figure 15: Comparison of the field production data to the simulation results for Michelle Ute well in east-side four-section model: a) cumulative oil production, b) cumulative gas production.

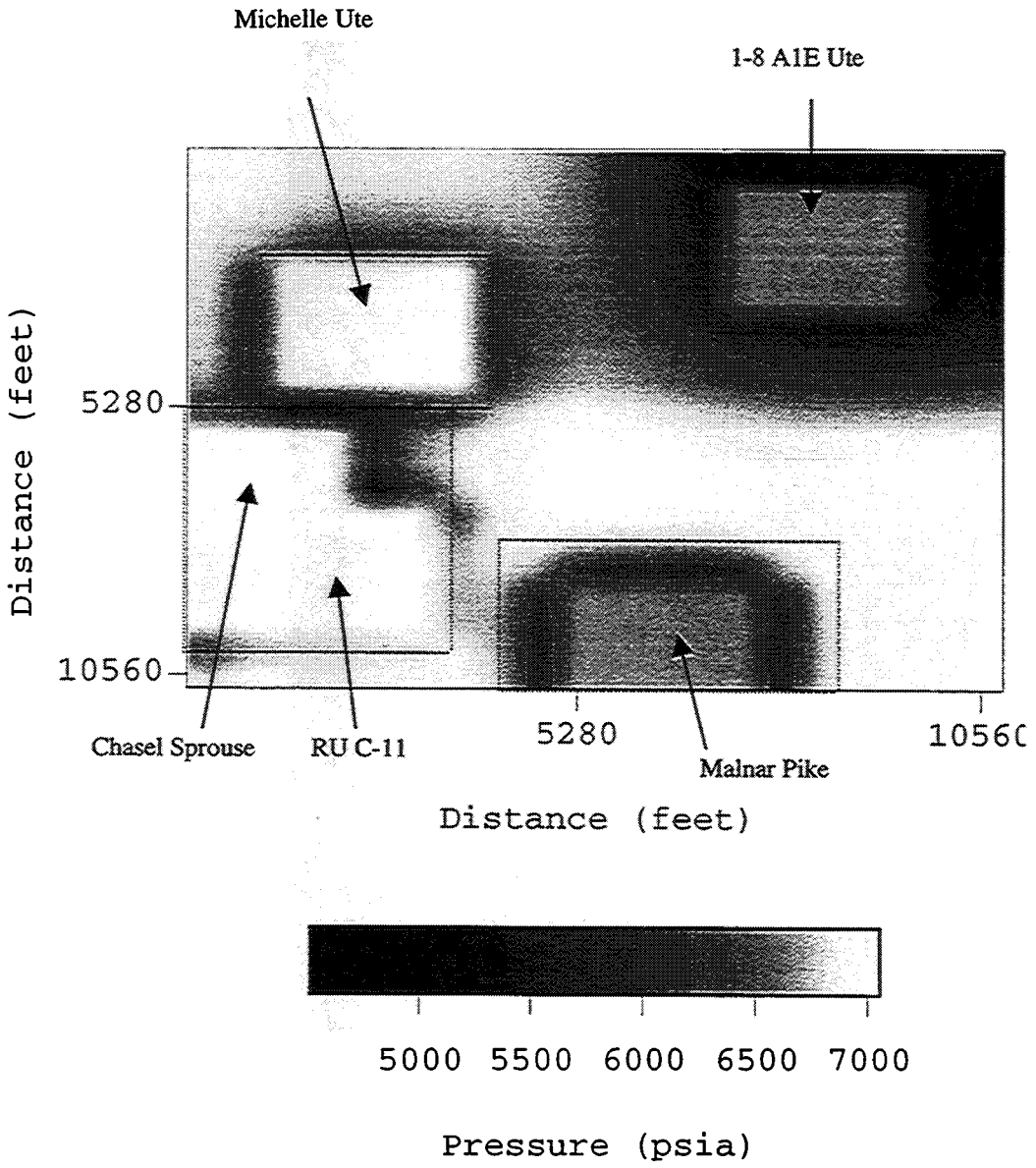

Figure 16: Pressure distribution throughout the east-side four-section area at the end of simulation.

a)

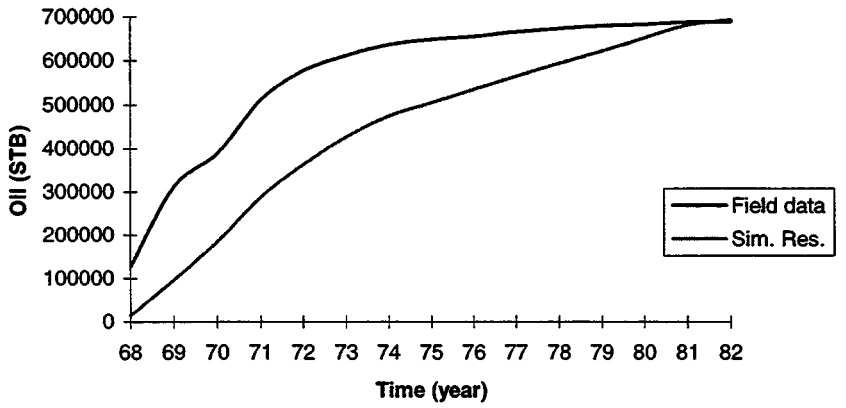

b)

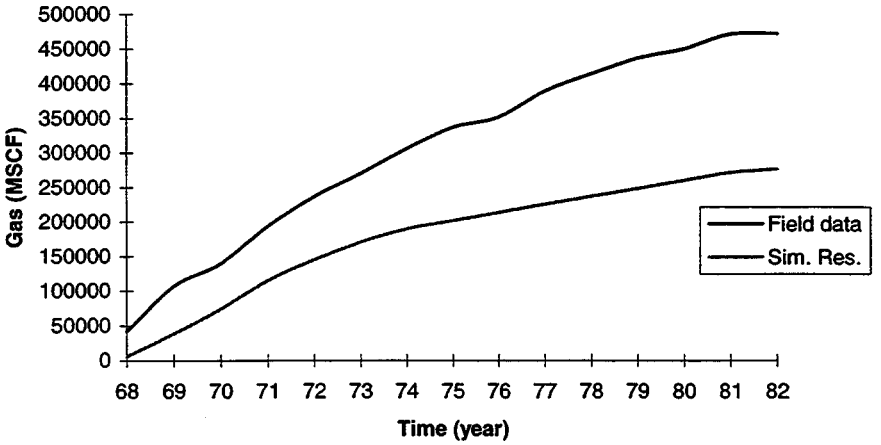

Figure 17: Production history match for the West side four section area model a) oil b) gas.

a)

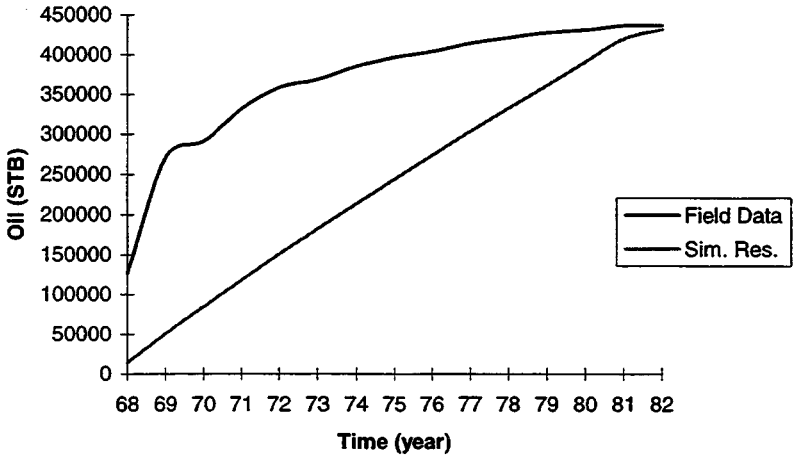

b)

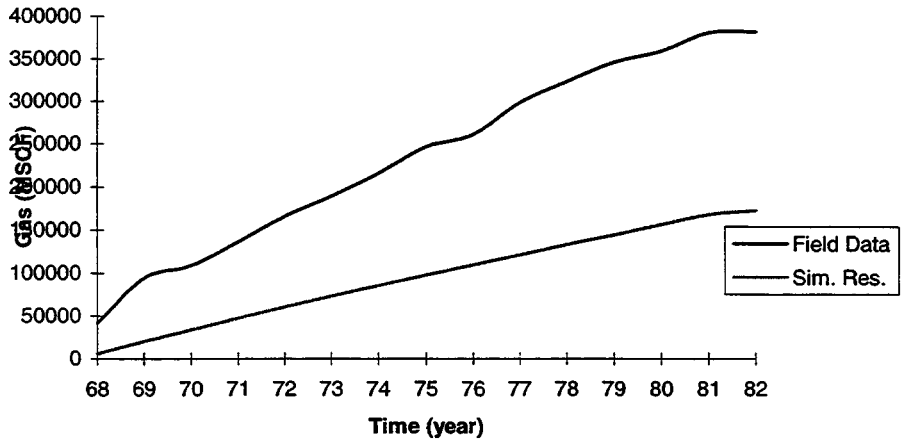

Figure 18: Production history match for well 3-10C a) oil b) gas.

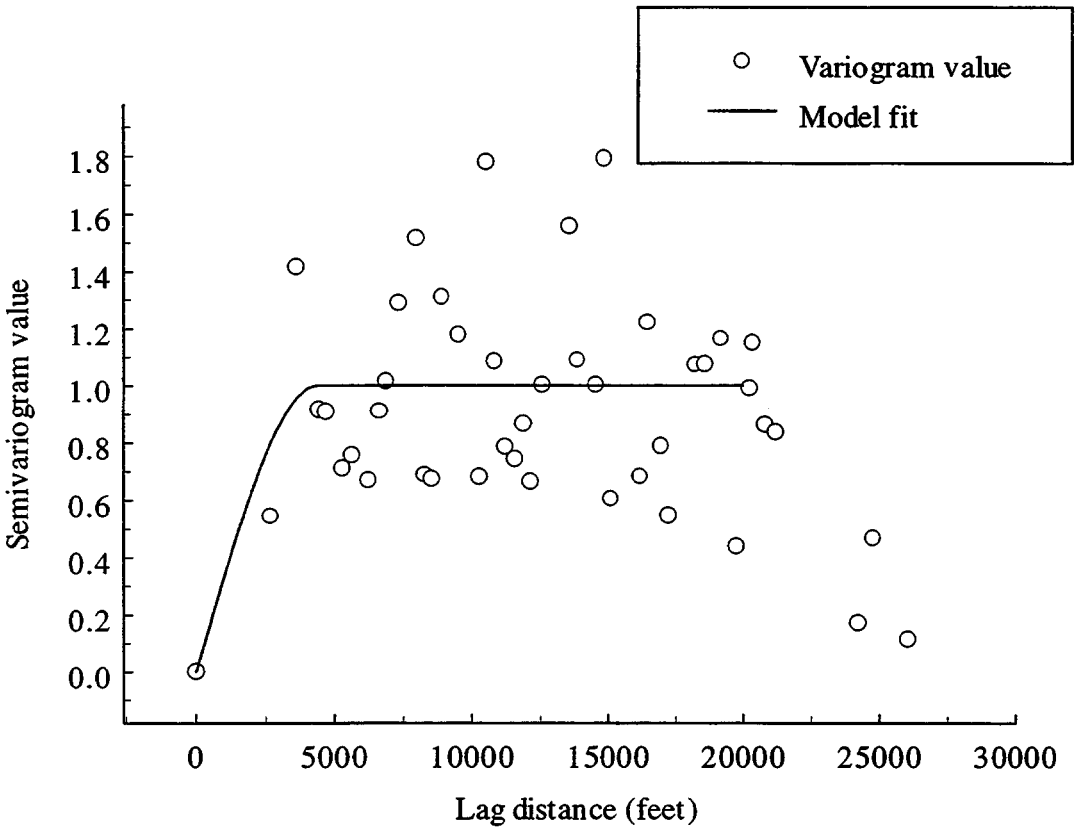

Figure 19: Semivariogram for thickness in bed 30.

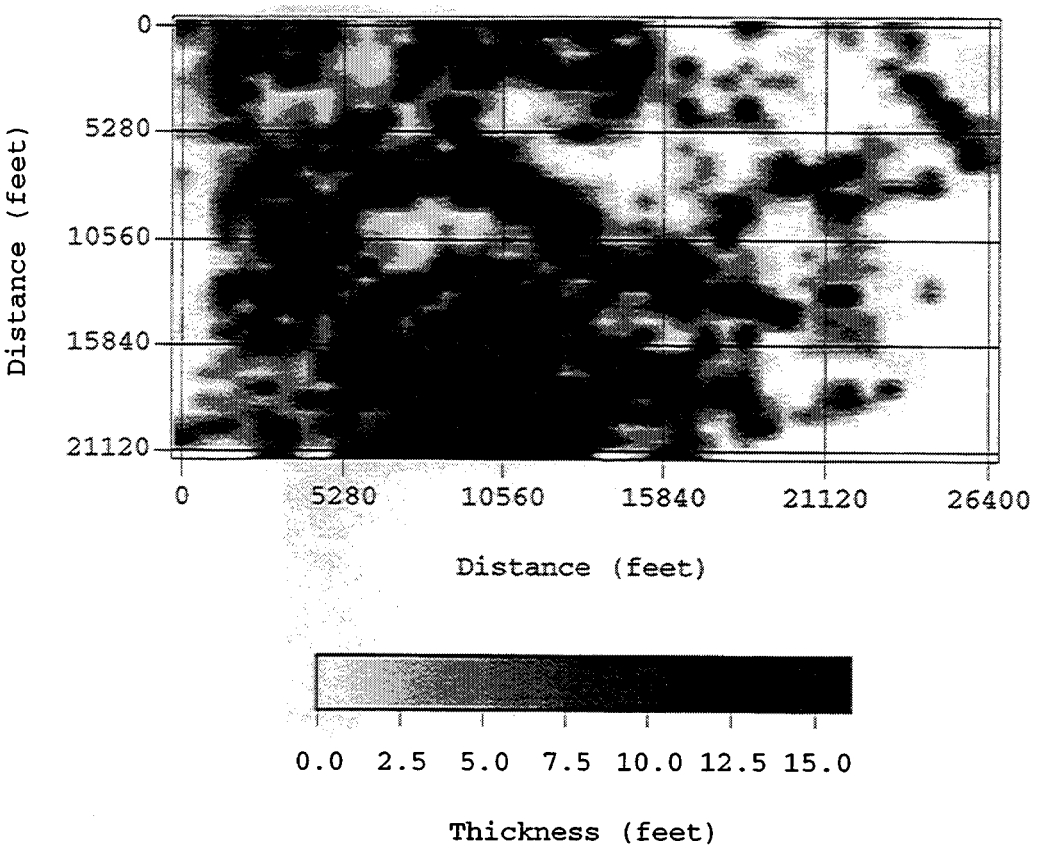

Figure 20: A realization of thickness in bed 30.

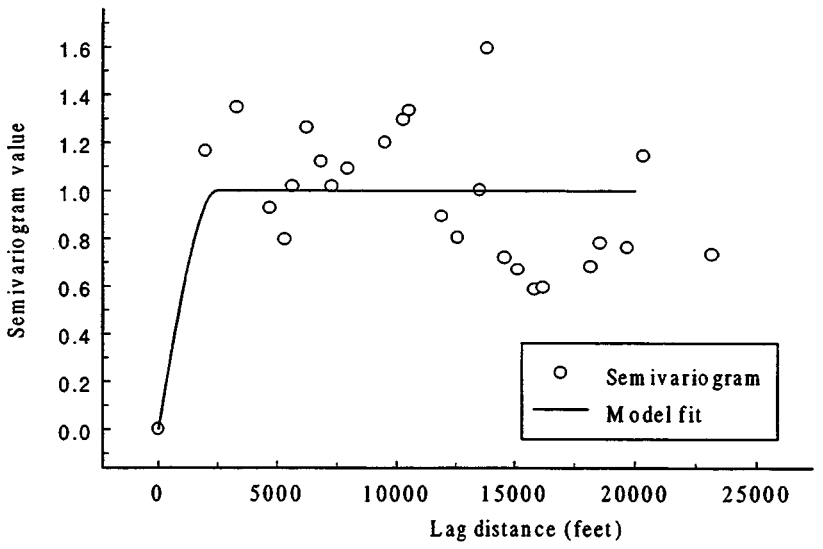

Figure 21: Semivariogram for porosity in bed 30.

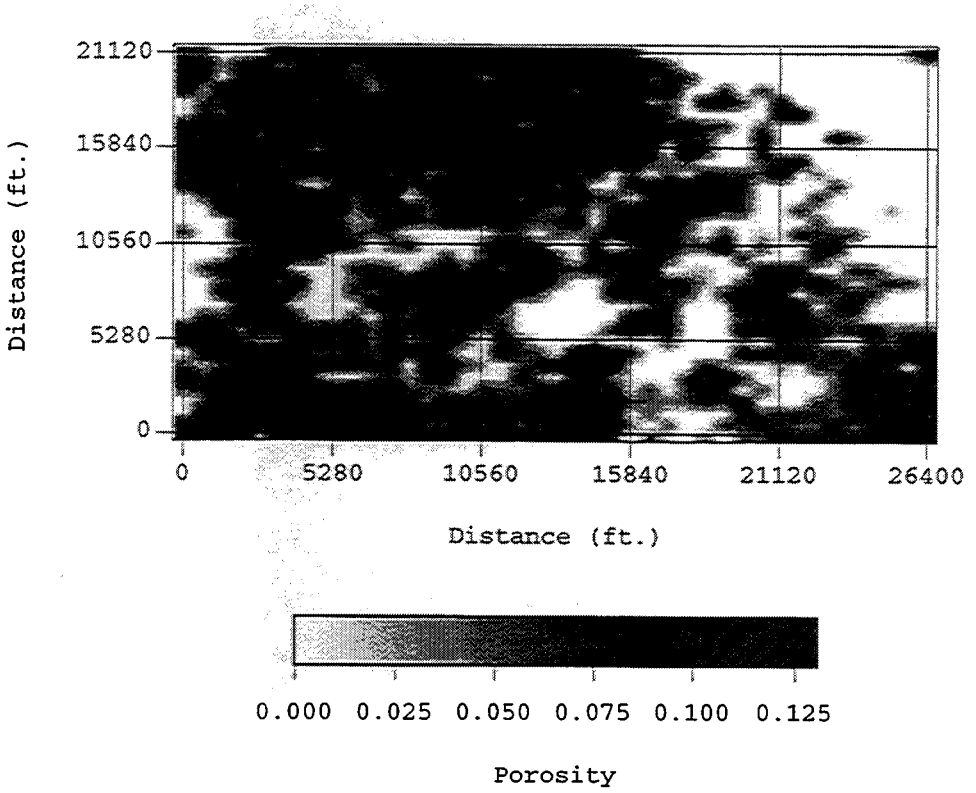

Figure 22: A realization of porosity in bed 30.

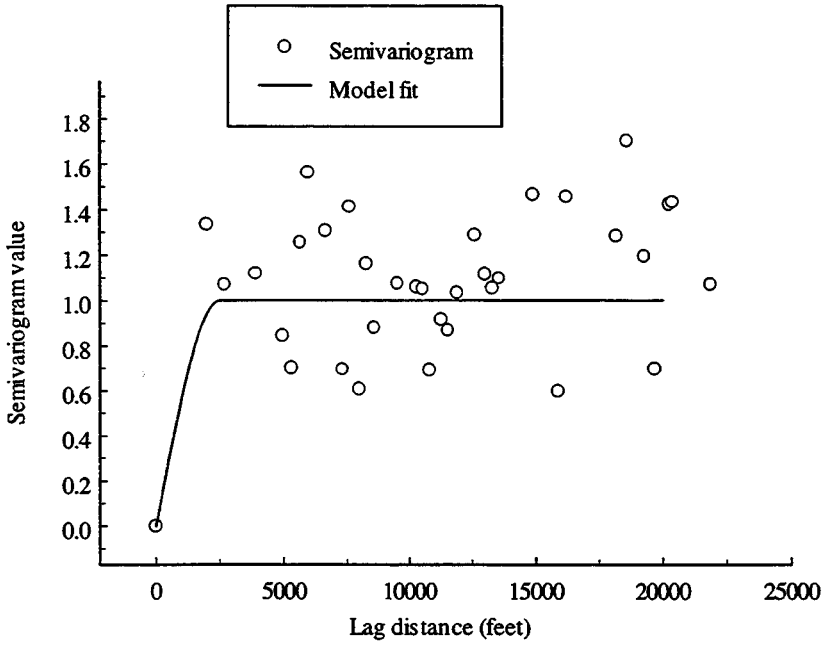

Figure 23: Semivariogram for saturation in bed 30.

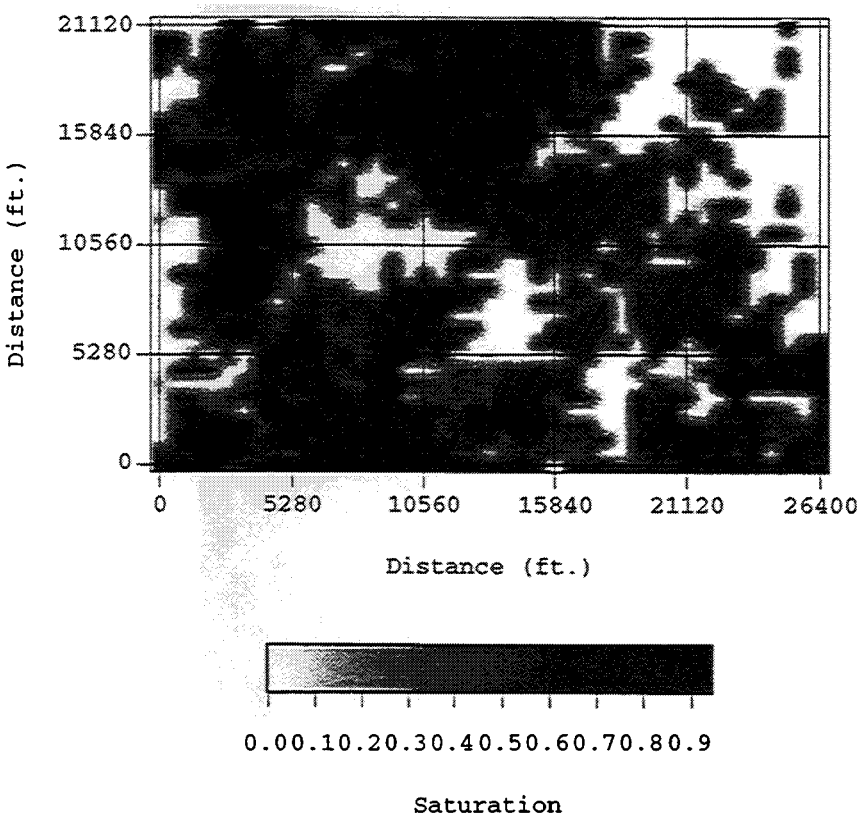

Figure 24: A saturation realization in bed 30.

a)

6180	6159	6104	6169	6184
5863	5579	5263	5814	6058
5427	4387	3134	5111	5831
5381	4988	4524	5210	5735
-	-	5071	5326	5607

Well block

b)

3421	2895	2713	2923	3499
3341	2413	2131	2435	3434
3322	2409	2088	2430	3420
3399	2420	2138	2442	3480
3516	3001	2829	3027	3583

Figure 26: Pressure distributions for well blocks surrounding Michelle Ute well: a) 20-section area model, b) single-well model.